Master’s Defense
December 20th, 2024

Mean Flow Characterization of Swept Shock/Turbulent Boundary Layer Interactions Induced by an Impinging Oblique Shock

Jesse Groves

Acknowledgements:
Dr. Jesse Little
Dr. James Threadgill
Dr. Alex Craig
Dr. Sathyan Padmanabhan
Max Vitols
Aaron Riley
AME Machine Shop
AFRL

The University of Arizona

Background

- Ferri (1939) was one of the first researchers to observed SBLI
- Shock/Boundary Layer Interactions (SBLI) are relevant in many applications
  - Control surfaces
  - Wings
  - Inlets and isolators
- Associated with:
  - Low frequency pressure fluctuations
  - Increased heat transfer
  - Flow separation

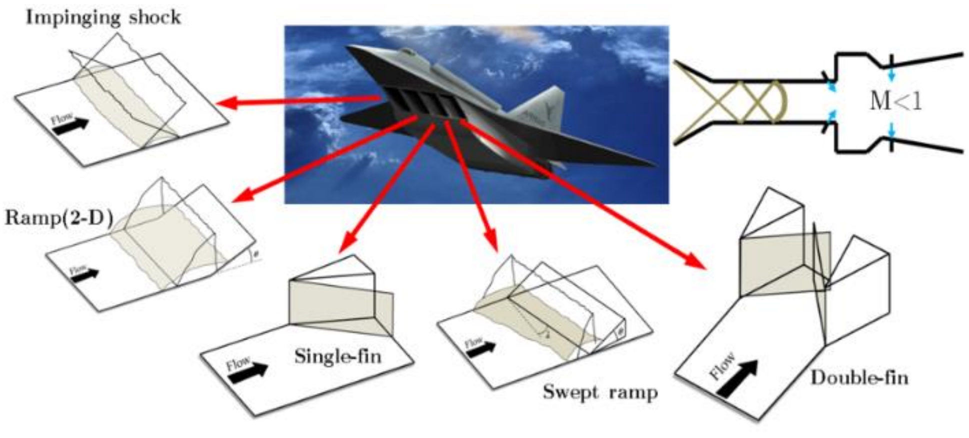

https://aapl.fsu.edu/projects/fsu-nal.html

https://en.wikipedia.org/wiki/North_American_X-15

Thompson, M. O. (2013). *At the edge of space: The X-15 flight program*. Smithsonian Books.

Shock Boundary Layer Interaction Features

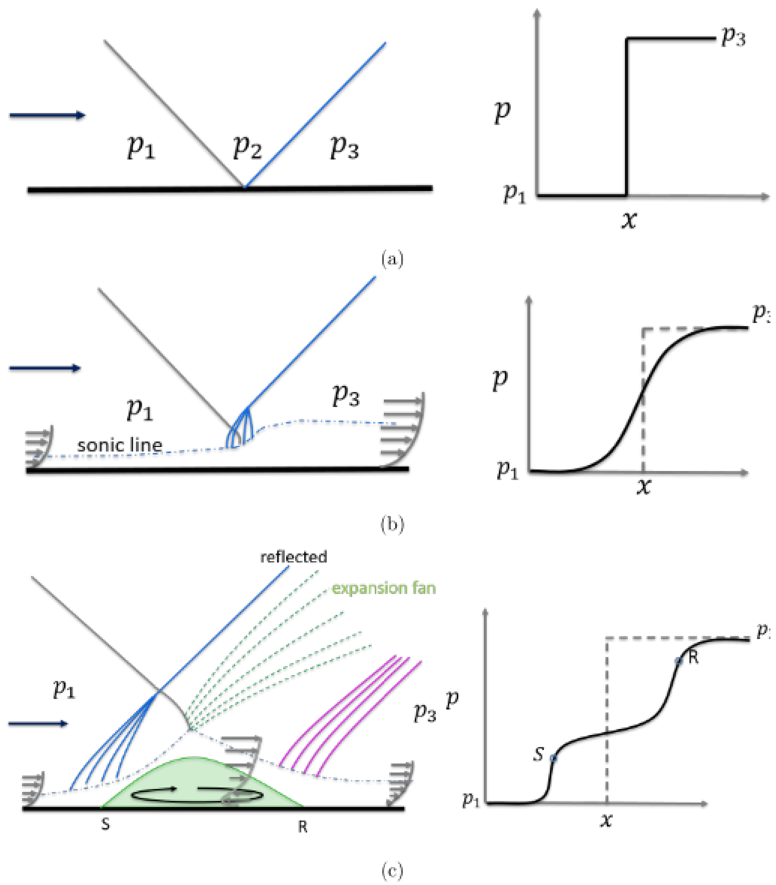

Padmanabhan (2023)

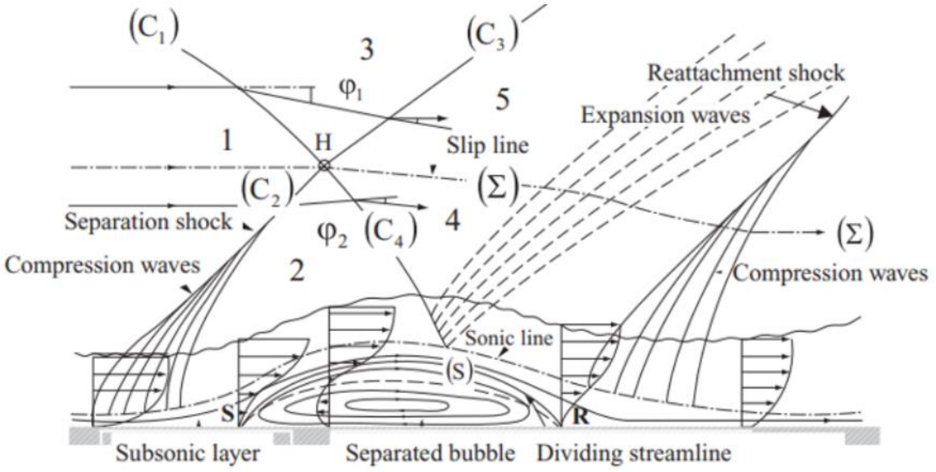

Delery and Dussauge (2009)

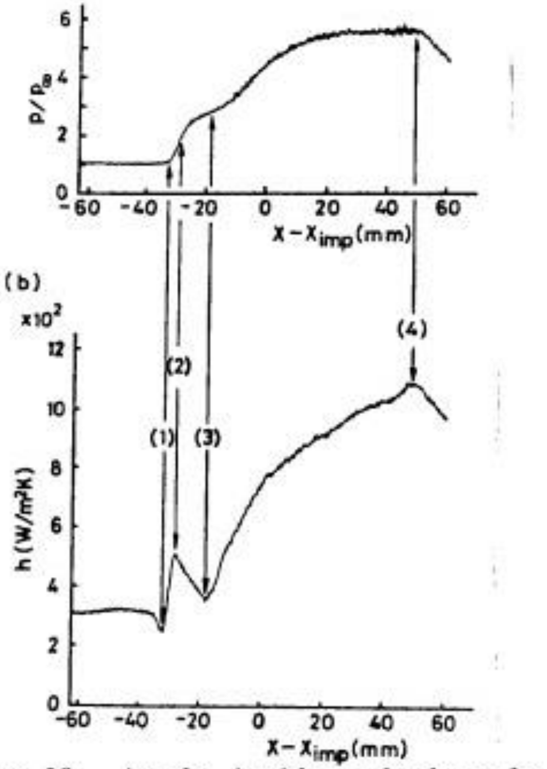

Figure 13. At the incident shock angle 22.1°
(a) pressure distribution (b) heat-transfer coefficient distribution

Hayashi (1986)

2-D vs 3-D Interactions

- 2-D interactions are constant in the z-direction
- 3-D interactions add a spanwise component of velocity
- Cylindrical vs conical interactions
  - Separation and reattachment lines are parallel for cylindrical interactions, and diverge for conical interactions

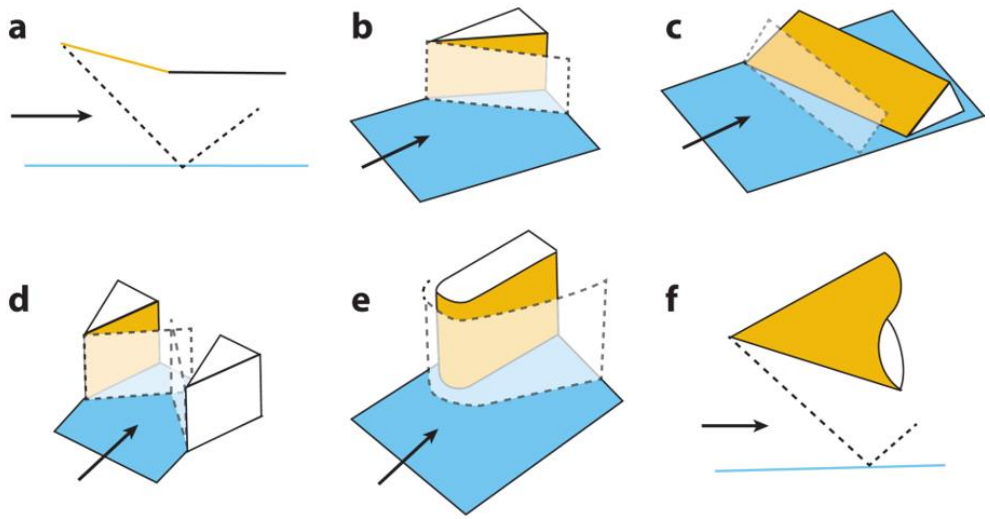

Gaitonde and Adler (2023)

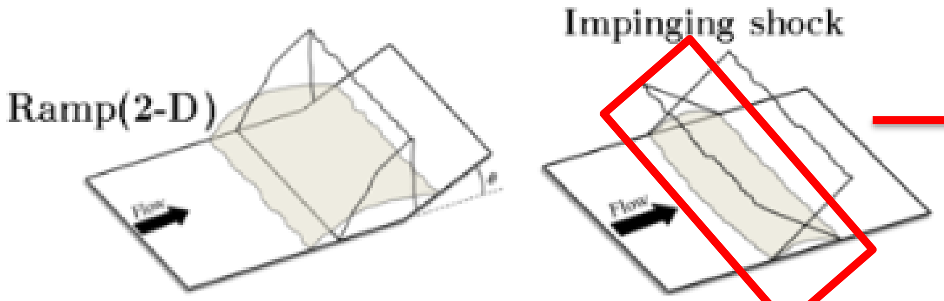

Gaitonde (2013)

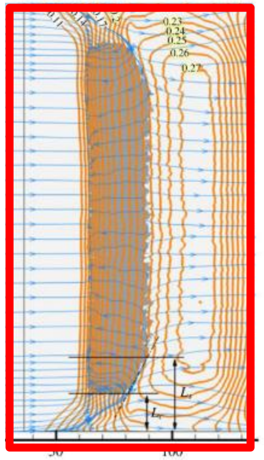

Wang et al. (2015)

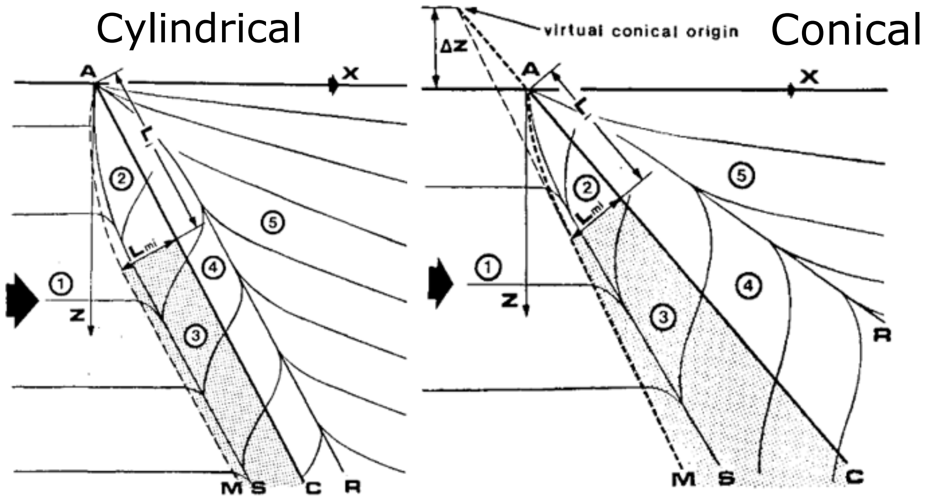

Settles and Teng (1984)

2-D Interactions

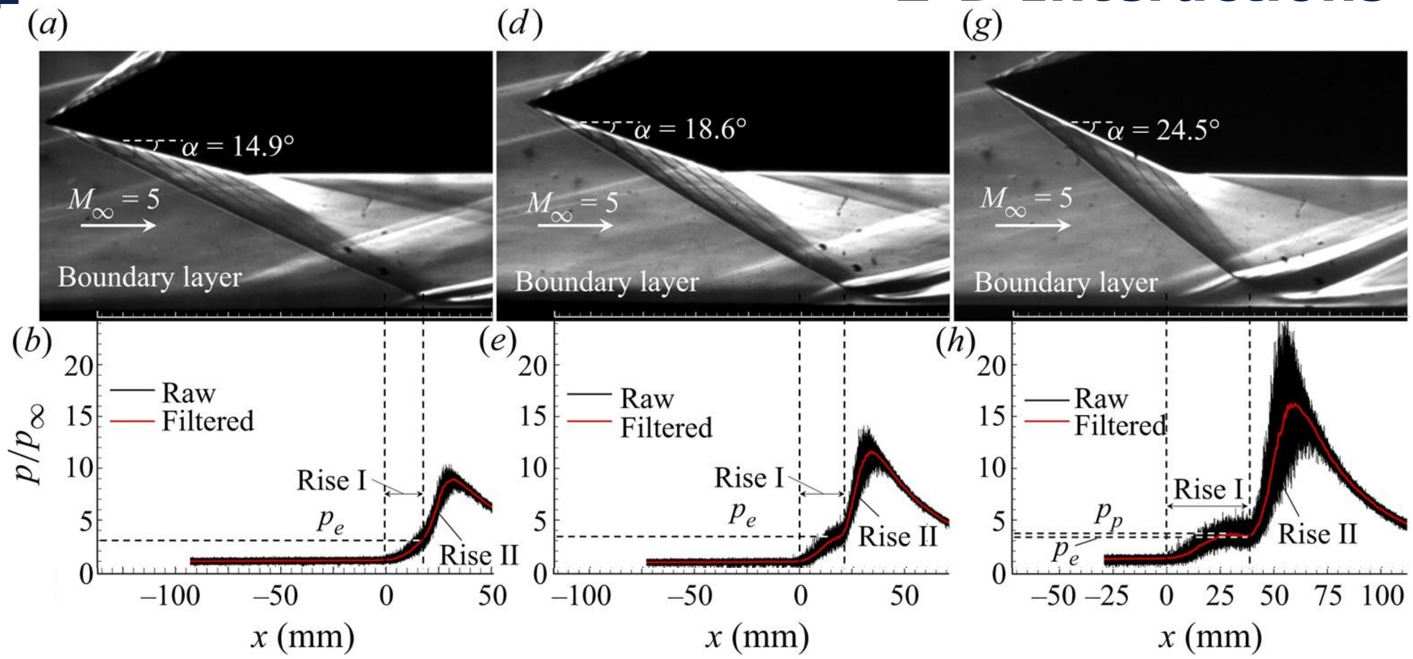

Xue et al. (2023)

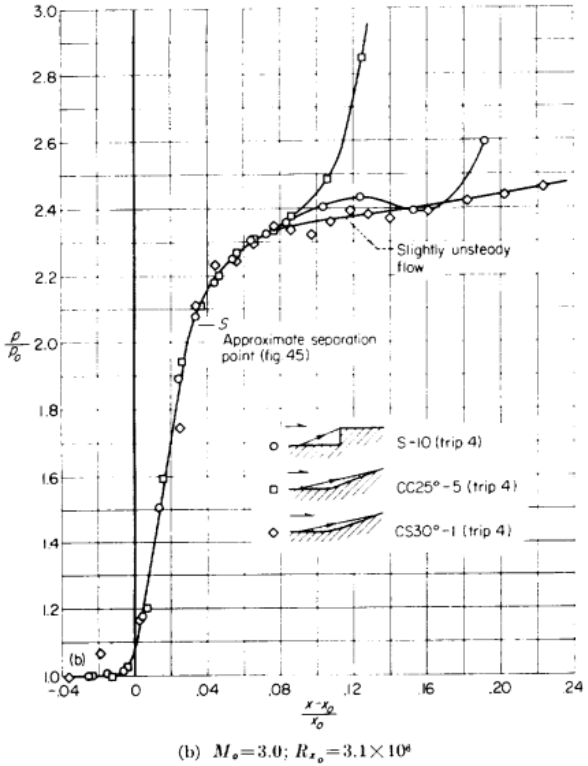

Chapman et al. (1958)

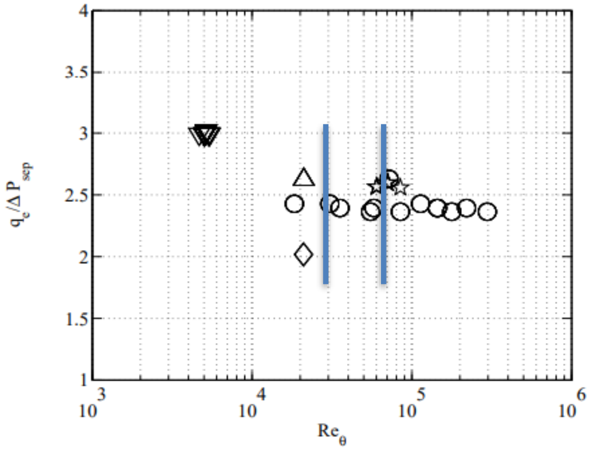

Souverein et al. (2013)

- Dimensionless geometries used to systematically study interactions
- Different aspects of flow that have been studied include:
  - Strength of pressure gradient
  - Mach number
  - Reynolds number
  - Boundary layer state
  - Interaction configuration
- Chapman et al. (1958) proposed Free Interaction Theory

3-D Interactions

- Settles and Teng (1984) attempted to determine a criterion for if flow will be cylindrically or conically separated
- Sidewall and shock generator tip effects can affect if this region is large enough for 3-D interactions
- Vanstone et al. 2018 argues inception region is larger for weakly separated flow
- Current investigation has sidewall and shock generator tip effects

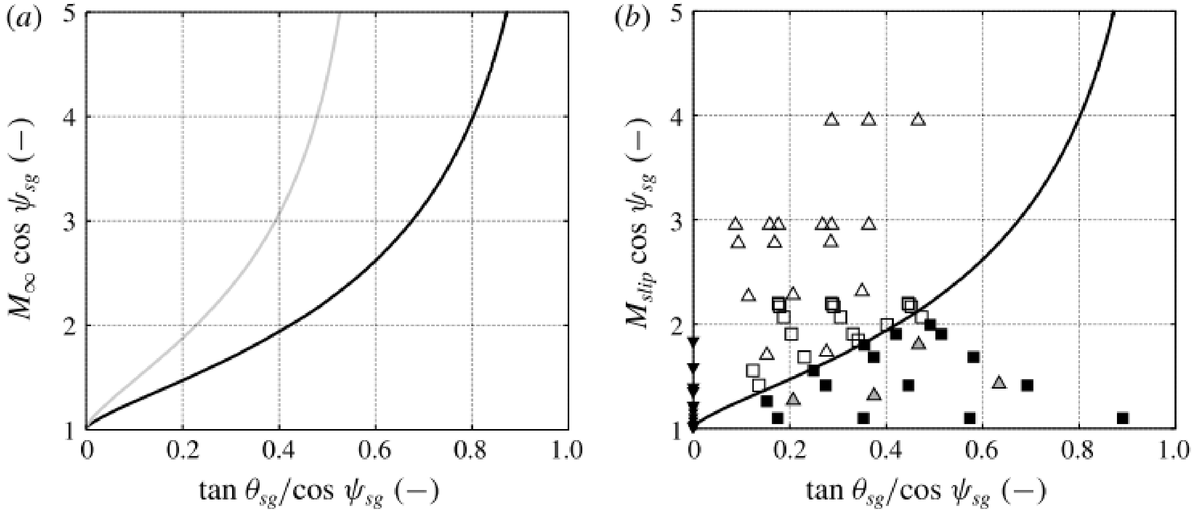

Threadgill and Little (2020)

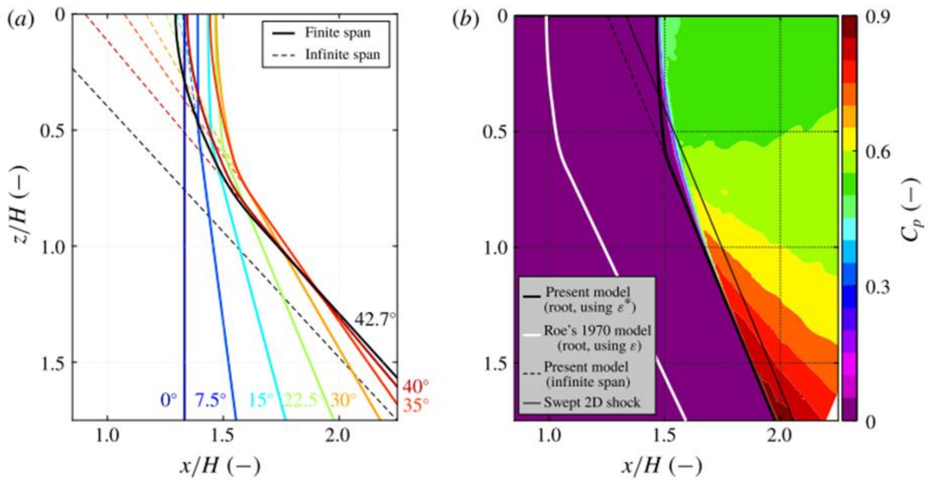

Threadgill and Little (2020)

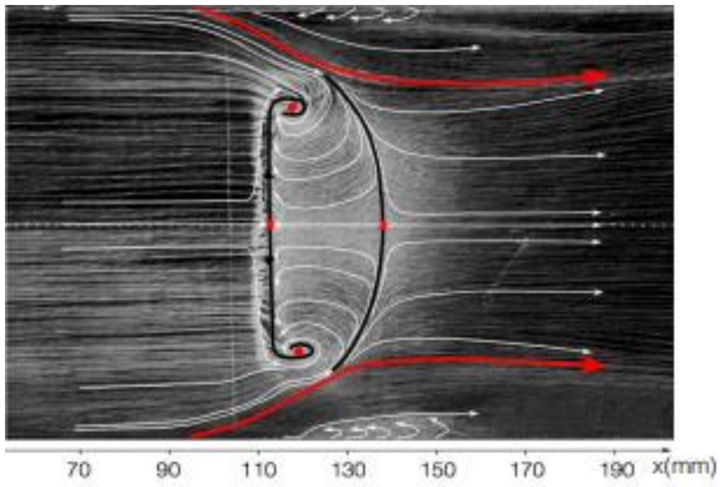

Xiang and Babinskey (2019)

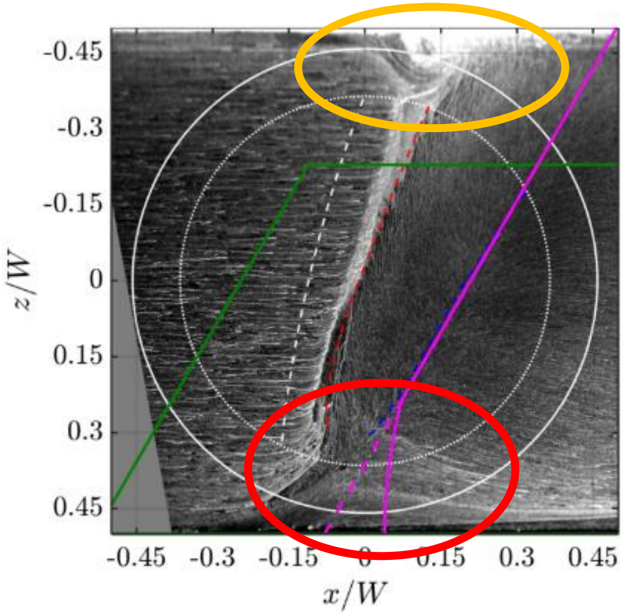

Padmanabhan (2024)

Swept Impinging Oblique SBLI

- Aspect ratio determines if the span is large enough to get useful data from the flow
- Work by Vitols (2024) attempted to isolate the effect of sweep for swept impinging SBLI
  - Accomplished by making normal pressure rise across shock constant

$$C_{p_n} = \frac{2}{\gamma {M_\infty}^2 cos^2\psi}\left(\frac{p}{p_\infty} - 1\right)$$

- Unit Reynolds number held constant at $9.99 \times 10^6\ {}^1/_m$
- Mach number of 2.3
- Mean pressure, oil flow visualization, and heat flux to characterize mean flow topology
- Aspect ratio (AR) of 2.33

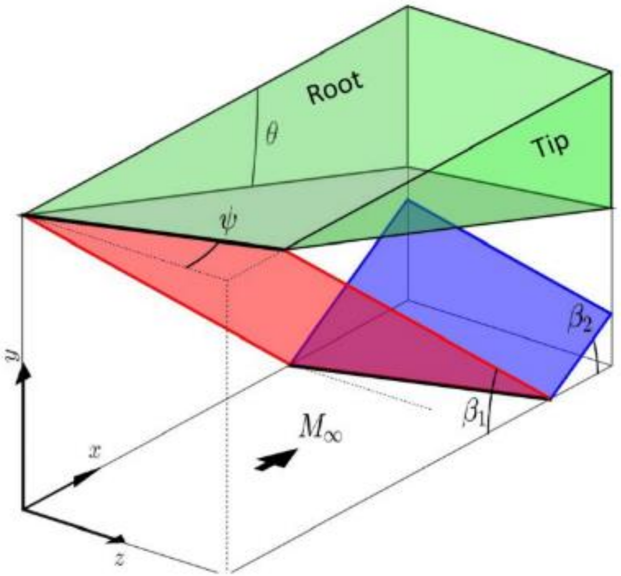

Threadgill and Little (2020)

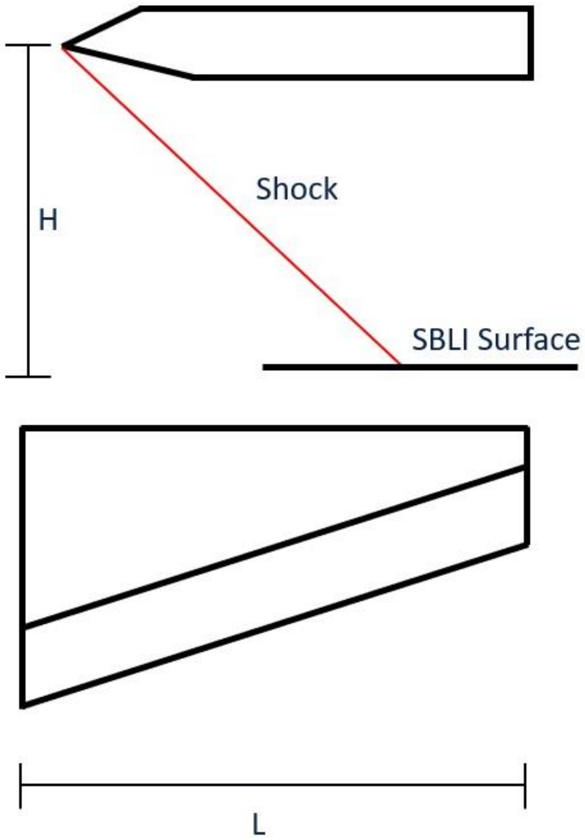

Mach, M	Pressure Coeff., Cpn	x-z shock generator sweep angle, Ψ				
		0°	10°	20°	30°	40°
2.3	0.4	8.04°	7.83°	7.22°	6.20°	4.80°
	0.6	10.64°	10.37°	9.59°	8.26°	6.36°
	0.8	12.73°	12.42°	11.48°	9.84°	7.37°

Swept Impinging Oblique SBLI

- Studying C_{p_n} rather than C_p shown to collapse the data between sweep cases
- Flow remains attached for some sweep value between 30° and 40° sweep
- Interactions shown to be conical

ψ	10°	20°	30°
Separation	9°	15°	22°
Reattachment	10°	18°	29°

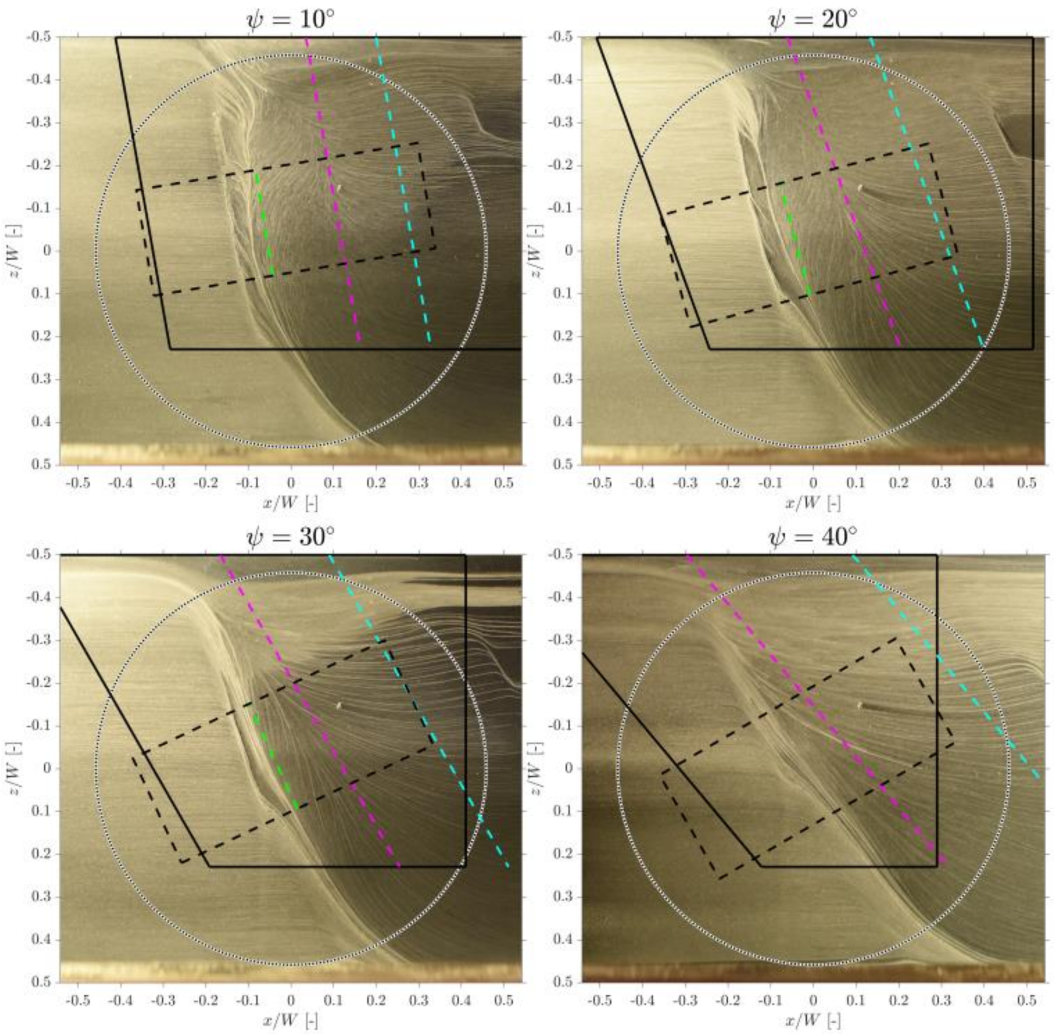

Vitols (2024)

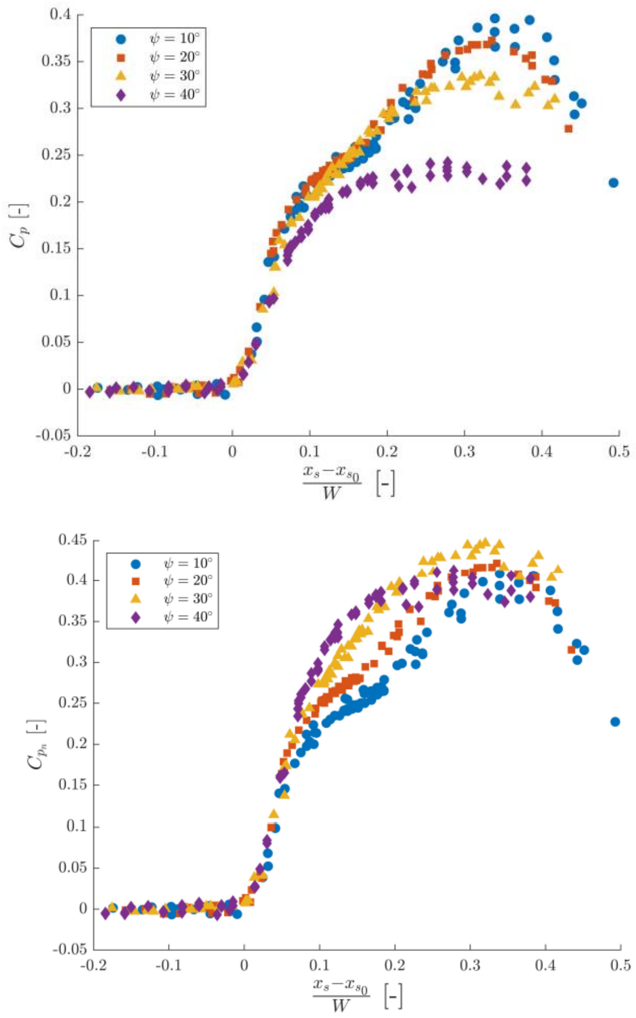

Vitols (2024)

Swept SBLI Heat Flux Measurements

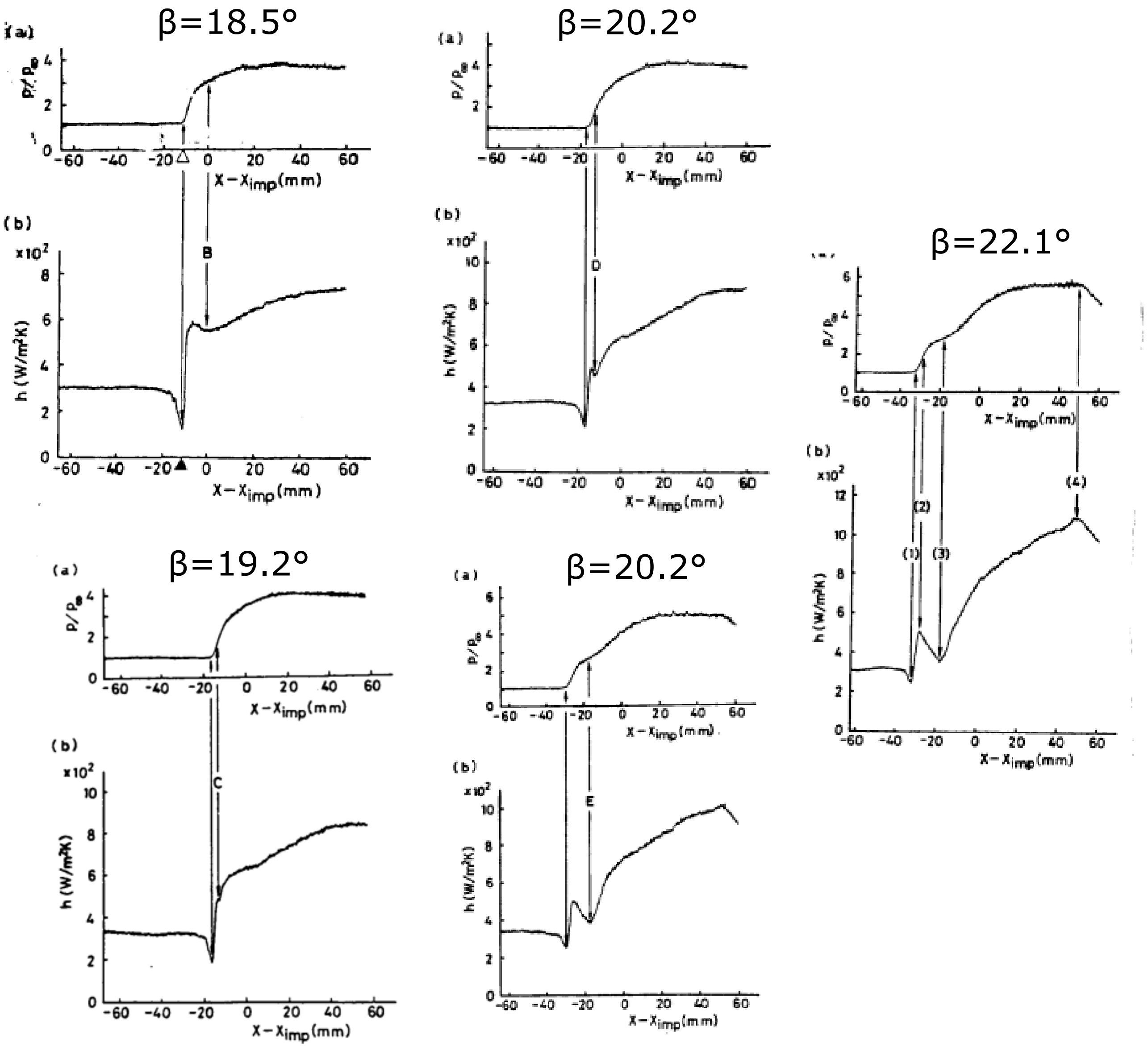

Hayashi et al. (1986)

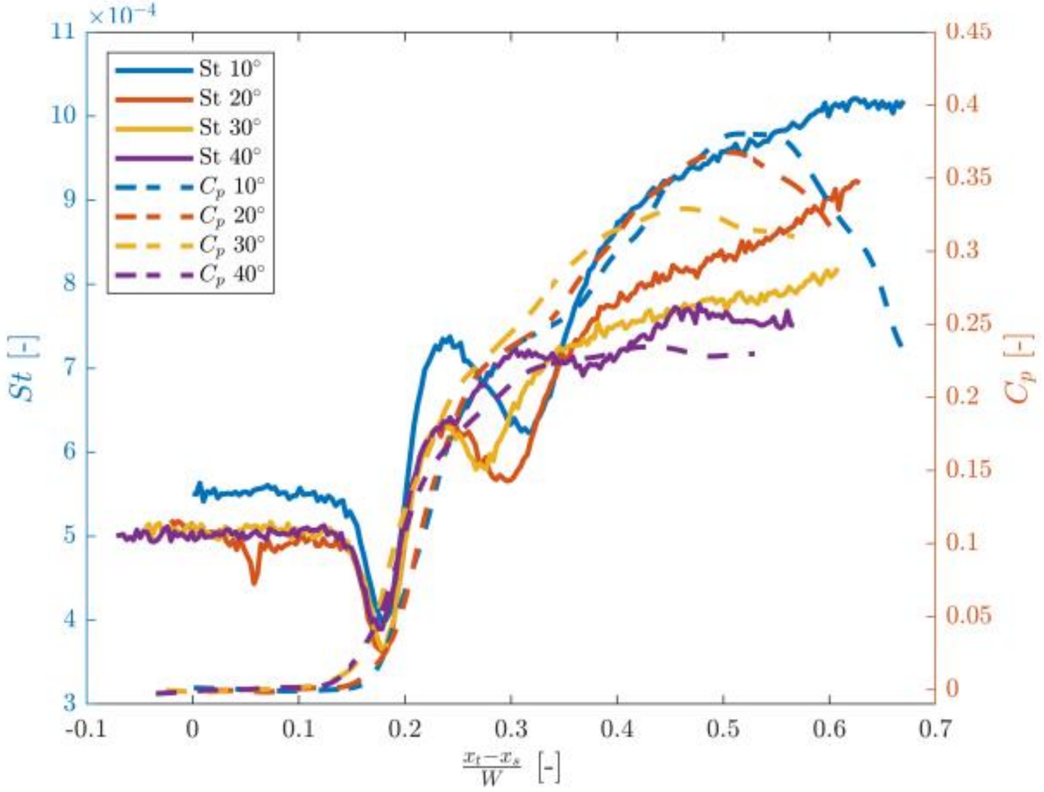

Vitols (2024)

Testing Matrix

- Testing in APWT conducted at:
  - Mach 2.1 and 3.0
  - 20° and 40° sweep cases
  - C_{p_n} = 0.6 and 0.41 for one case
  - AR = 2.75
- Reynolds numbers between $2.75 \times 10^7\ ^1/_m$ and $5.25 \times 10^7\ ^1/_m$ for all cases
- Mean flow characterization using:
  - Infrared thermography
  - Oil flow visualization
  - Mean pressure measurements
- Supporting tests conducted in ISWT had the following properties:
  - Mach 2.3
  - 20° and 40° sweep cases
  - C_{p_n} = 0.6
  - AR = 2.33

Mach, M	Pressure Coeff., C_{pn}	x-z shock generator sweep angle, ψ				
		0°	10°	20°	30°	40°
2.1	0.4	7.50°	7.29°	6.66°	5.63°	4.21°
	0.6	9.96°	9.69°	8.87°	7.49°	5.47°
	0.8	11.91°	11.57°	10.55°	8.76°	-
3.0	0.4	9.27°	9.07°	8.49°	7.52°	6.17°
	0.6	11.98°	11.74°	11.04°	9.86°	8.18°
	0.8	14.20°	13.94°	13.15°	11.79°	9.81°
4.0	0.4	10.04°	9.86°	9.33°	8.44°	7.18°
	0.6	12.63°	12.43°	11.81°	10.77°	9.29°
	0.8	14.76°	14.54°	13.86°	12.70°	11.03°

M_∞	2.1		3.0		
ψ	20	40	20		40
C_{p_n}	0.6	0.6	0.4	0.6	0.6
Oil	✓	✓			
Mean Pressure	✓	✓	✓*	✓	✓
IR	✓	✓	✓	✓	✓

*Mean pressure data for this case is more course than other cases.

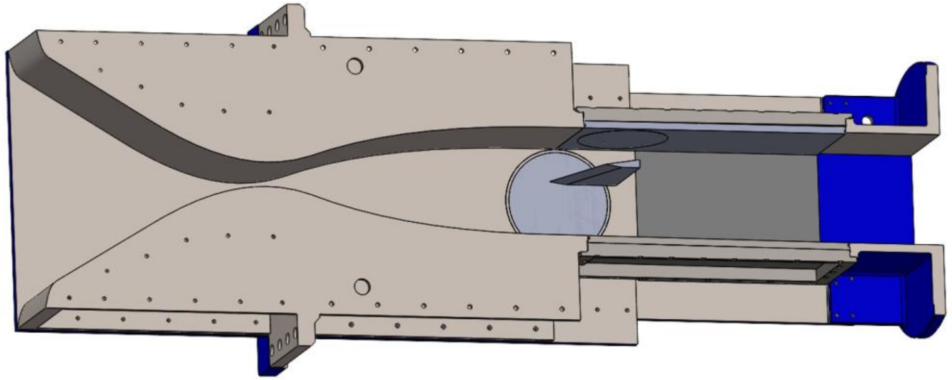

Boundary Layer Characterization

- Velocity profile determined using Rayleigh Pitot tube formula and the Crocco-Busemann temperature-velocity relationship
- Sun and Childs (1973) method used for upper profile and Spalding (1970) for lower profile
- Boundary layer of SBLI surface in APWT characterized as fully turbulent

Tunnel	M_∞ [-]	$u_\infty [\frac{m}{s}]$	δ [mm]	δ^* [mm]	θ [mm]	H [-]	C_f [-]	Re_∞/L [$\frac{1}{m}$]
APWT	2.07	516	15.25	5.58	1.01	5.50 (1.3)	3×10^{-3}	2.80×10^{7}
ISWT	2.28	554.8	6.53	2.03	0.56	3.66 (1.39)	2.00×10^{-3}	9.99×10^{6}

$$\frac{\bar{T}}{T_\infty} = \frac{T_w}{T_\infty} + \left[1 + r\frac{\gamma-1}{2}{M_\infty}^2 - \frac{T_w}{T_\infty}\right]\frac{\bar{u}}{u_\infty} - r\frac{\gamma-1}{2}{M_\infty}^2\left(\frac{\bar{u}}{u_\infty}\right)^2$$

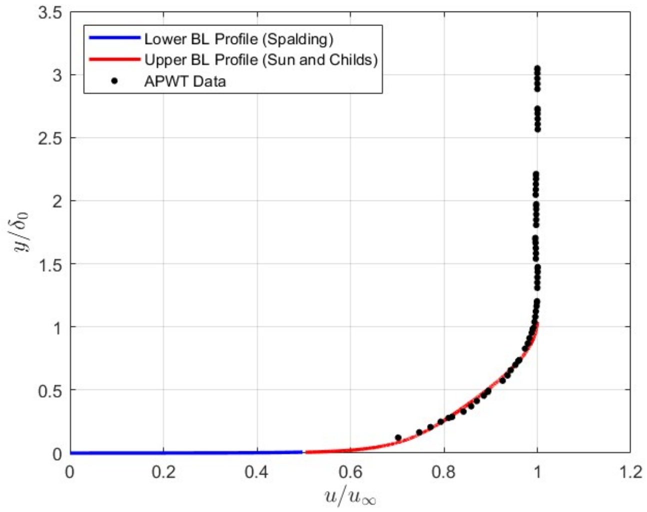

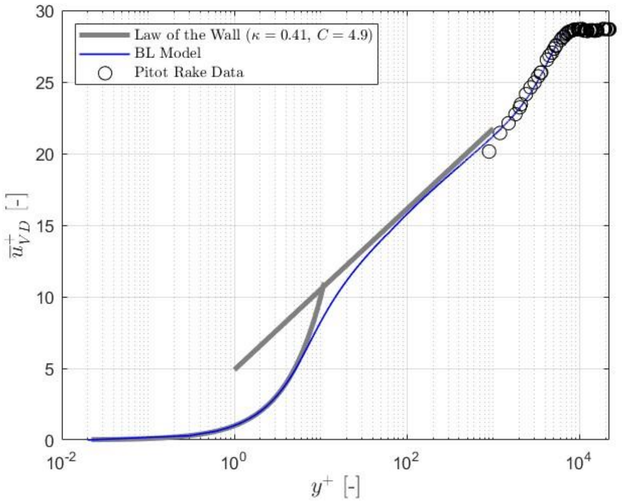

Mean Pressure Setup

- 8 total runs to map entire plug
  - 47 sensors per run for 369 data points
- Results mapped to a grid and smoothed with Gaussian kernel smoothing
  - Kernel value of 0.3 chosen
- Interpolated results provide initial pressure rise line by using a threshold of $C_{p_n} = 0.03$
  - All other data take only from data points

M_∞ [-]	2.1		3.0		
ψ [°]	20	40	20		40
p_0 [psi]	45	45	90		88
$\frac{Re}{L}^*$ $[\frac{1}{m}]$	4.05×10^7	3.96×10^7	8.40×10^7	8.31×10^7	7.93×10^7
C_{p_n} [-]	0.6	0.6	0.4	0.6	0.6
C_p [-]	0.5298	0.3521	0.3532	0.5298	0.3521
θ_{sg}	8.87°	5.47°	8.87°	11.04°	8.18°

*Reynolds numbers averaged over run due to changing total temperature.

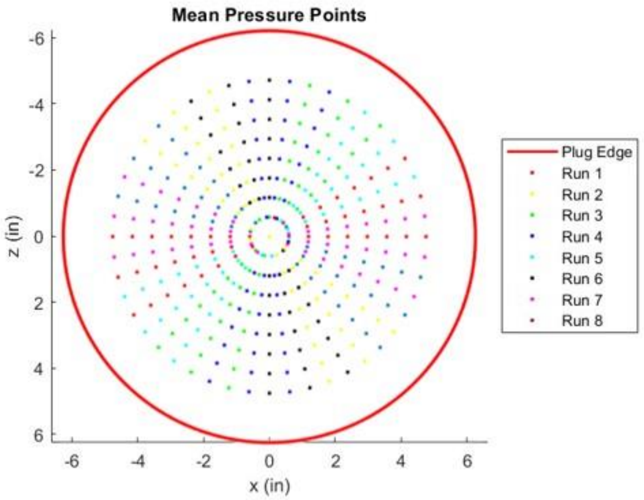

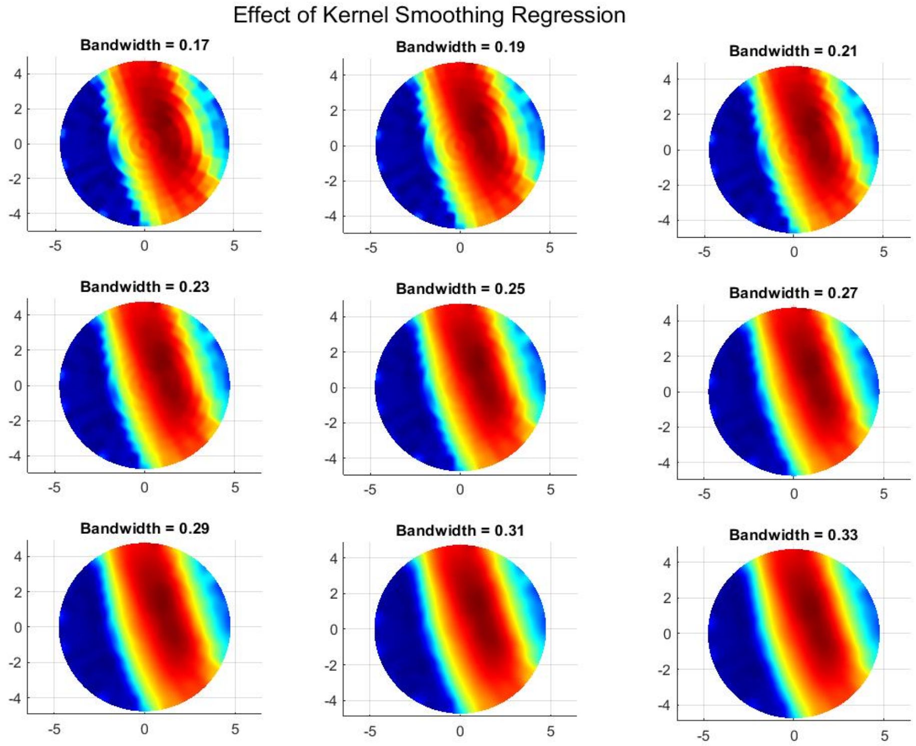

Infrared (IR) Thermography Setup

- Camera put through three calibrations:
  - Sensor calibration
  - Experimental calibration
  - Sensor drift correction
- Experimental calibration uses Planck's Law to convert counts to radiance
- IR camera looks through sapphire window to PEEK plug
- Rataczak et al. (2021) and Franklin et al. (2024) show that PEEK can be assumed opaque
  - Temperature measured by camera is assumed to be true surface temperature

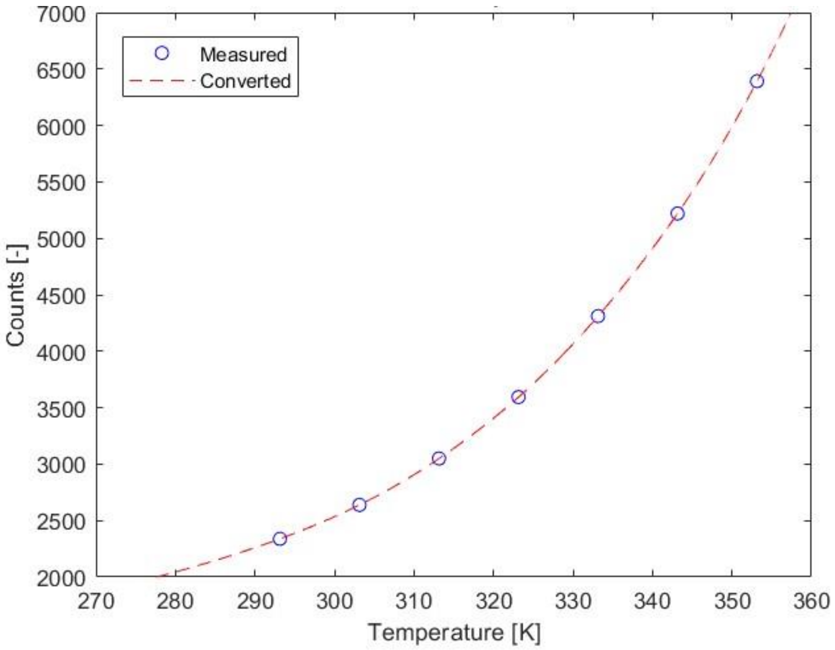

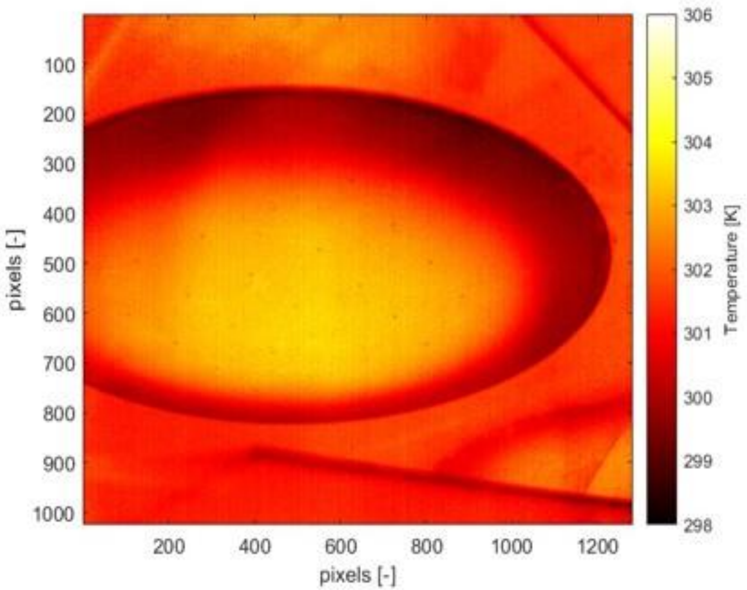

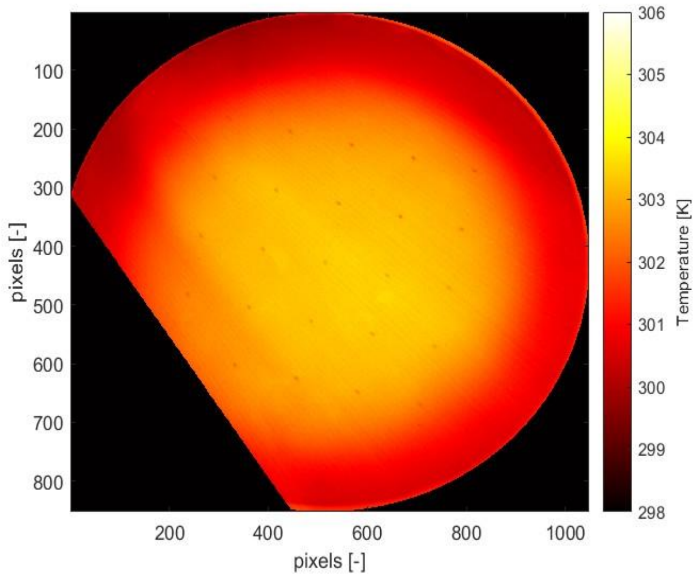

Infrared Thermography Setup

- Heater used to improve signal-to-noise ratio
- 1-D heat transfer equation used to solve heat flux and Stanton number
  - Heat transfer is really 2-D

M_∞ [-]	2.1				3.0		
ψ [°]	20		40		20		40
p_0 [psi]	30	50	30	50	100	100	100
C_{p_n} [-]	0.6	0.6	0.6	0.6	0.4	0.6	0.6
C_p [-]	0.5298	0.5298	0.3521	0.3521	0.3532	0.5298	0.3521
θ_{sg}	8.87°	8.87°	5.47°	5.47°	8.87°	11.04°	8.18°
T_w [K]	Unheated 30 50 80 100	Unheated 30 50 80 100	Unheated 30 50 80 100	Unheated 30 50 80 100	30 50 80	30 50 80	30 50 80

*Reynolds numbers averaged over run due to changing total temperature.

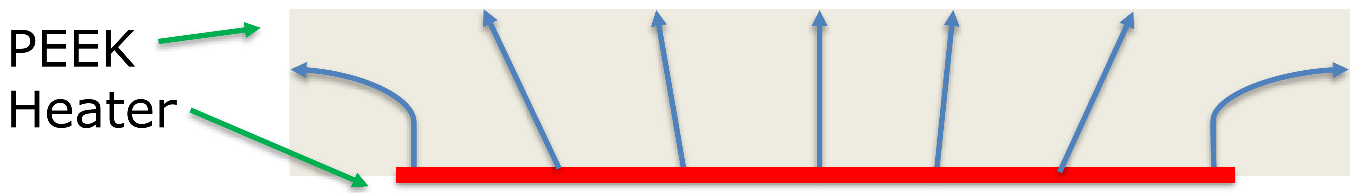

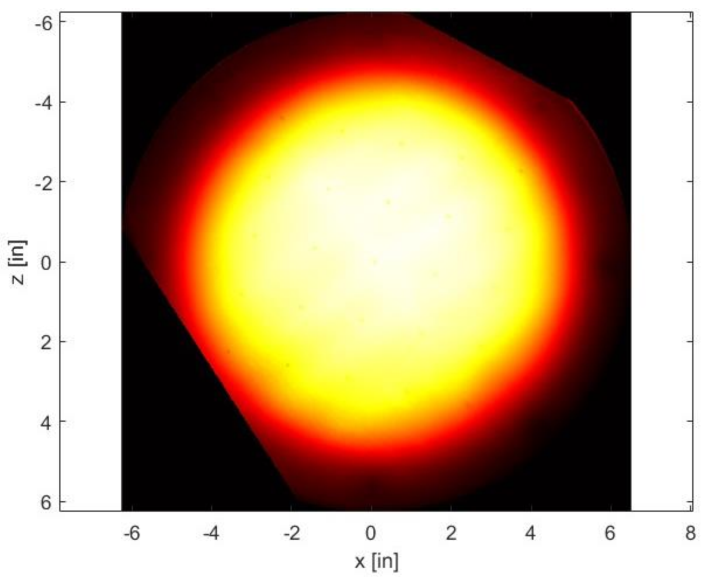

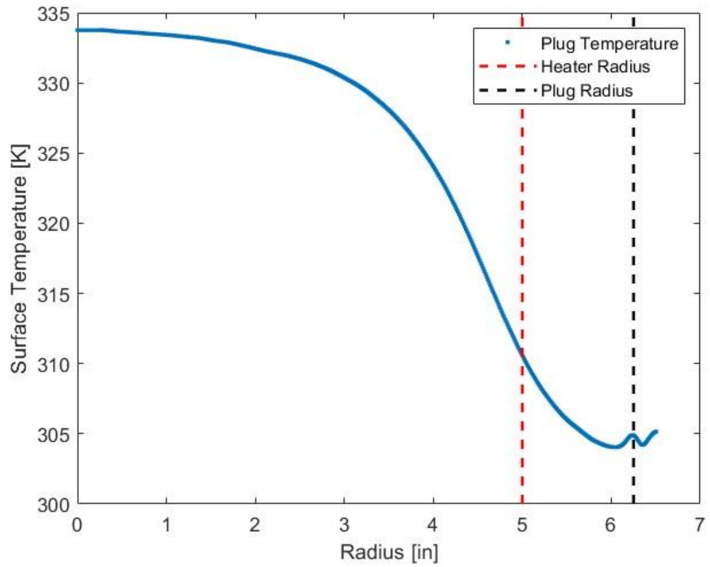

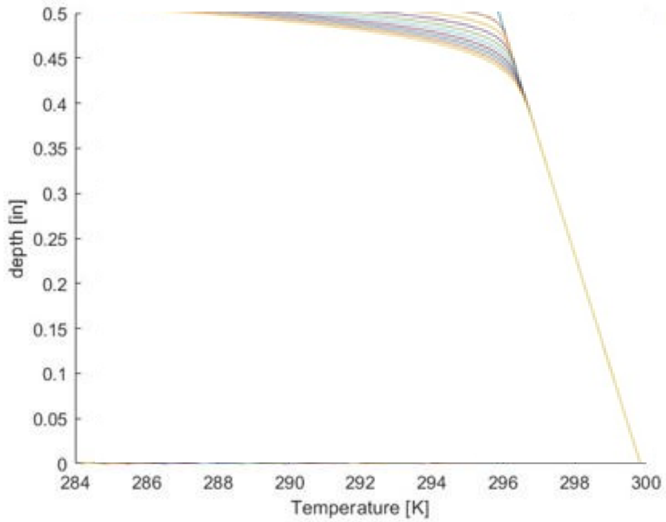

Adiabatic Wall Temperature

- Multiple temperatures utilized to get adiabatic wall temperature
- Adiabatic wall temperature determined from extrapolating temperature ratio that results in zero heat flux
- Mach 2.1 data missing total temperature
  - Total temperature for each test estimated using a recovery factor of 0.896 in the boundary layer
- Recovery factor found to be 0.91 for Mach 3.0

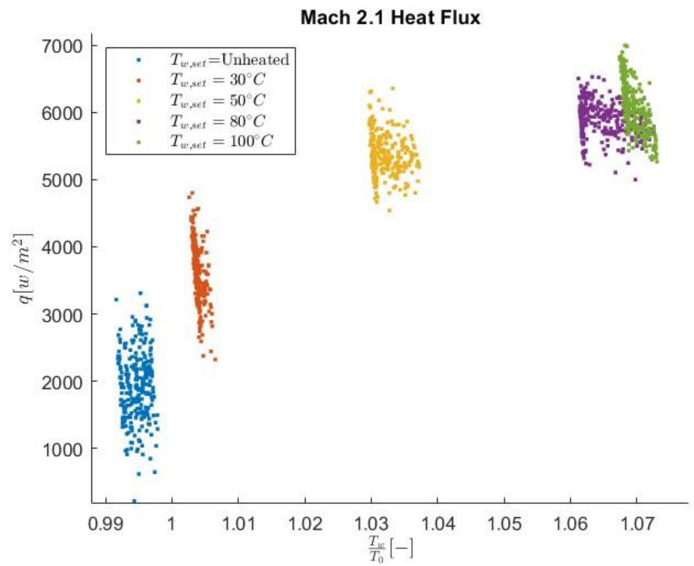

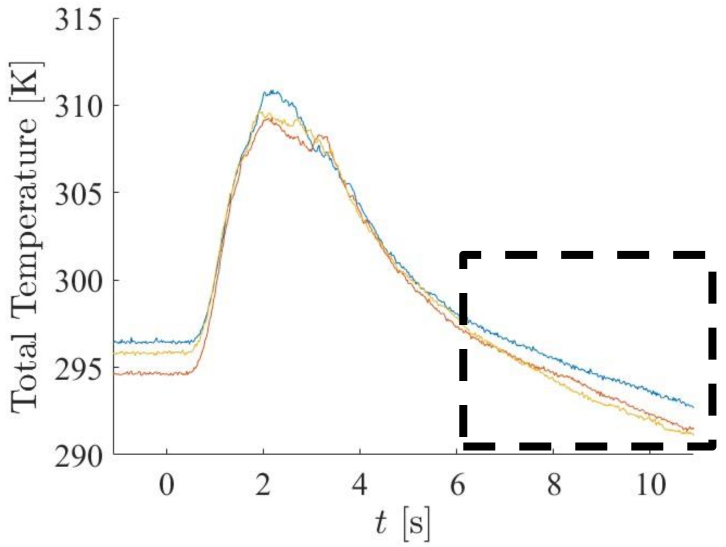

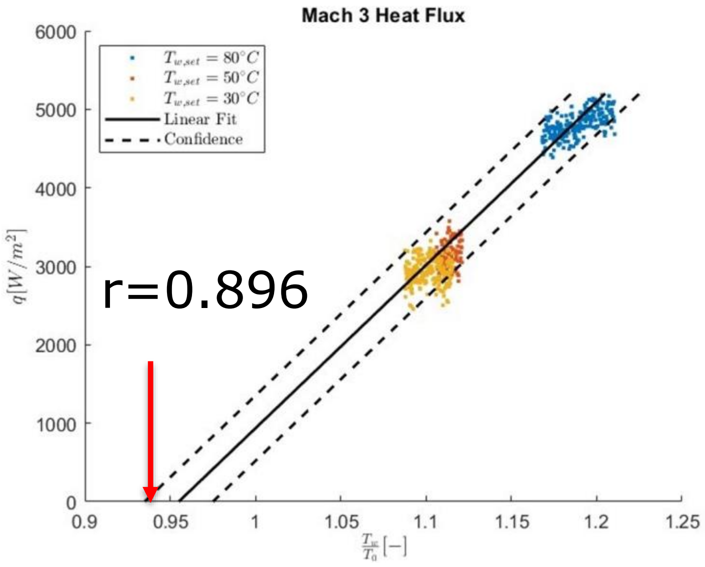

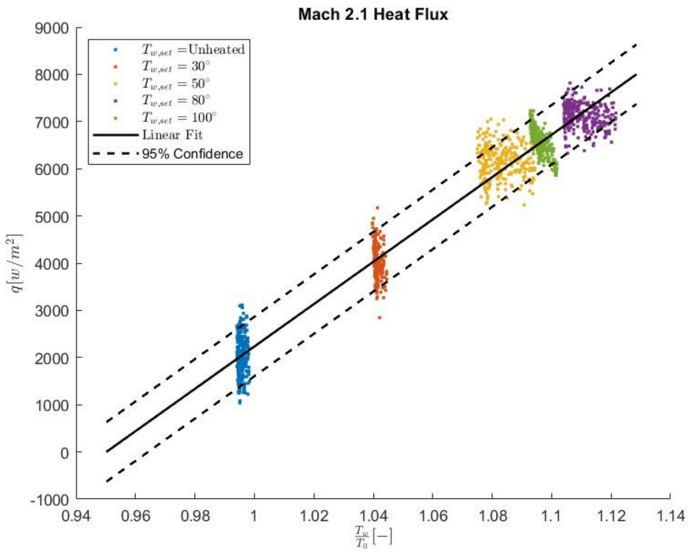

Oil Flow Visualization

- Mixture of kerosene, TiO_2, and oleic acid
- Oil flow conducted for Mach 2.1 flow, 20° and 40° sweep cases
- Two methods to study results
  - Hand picked points
  - Streak evaluation

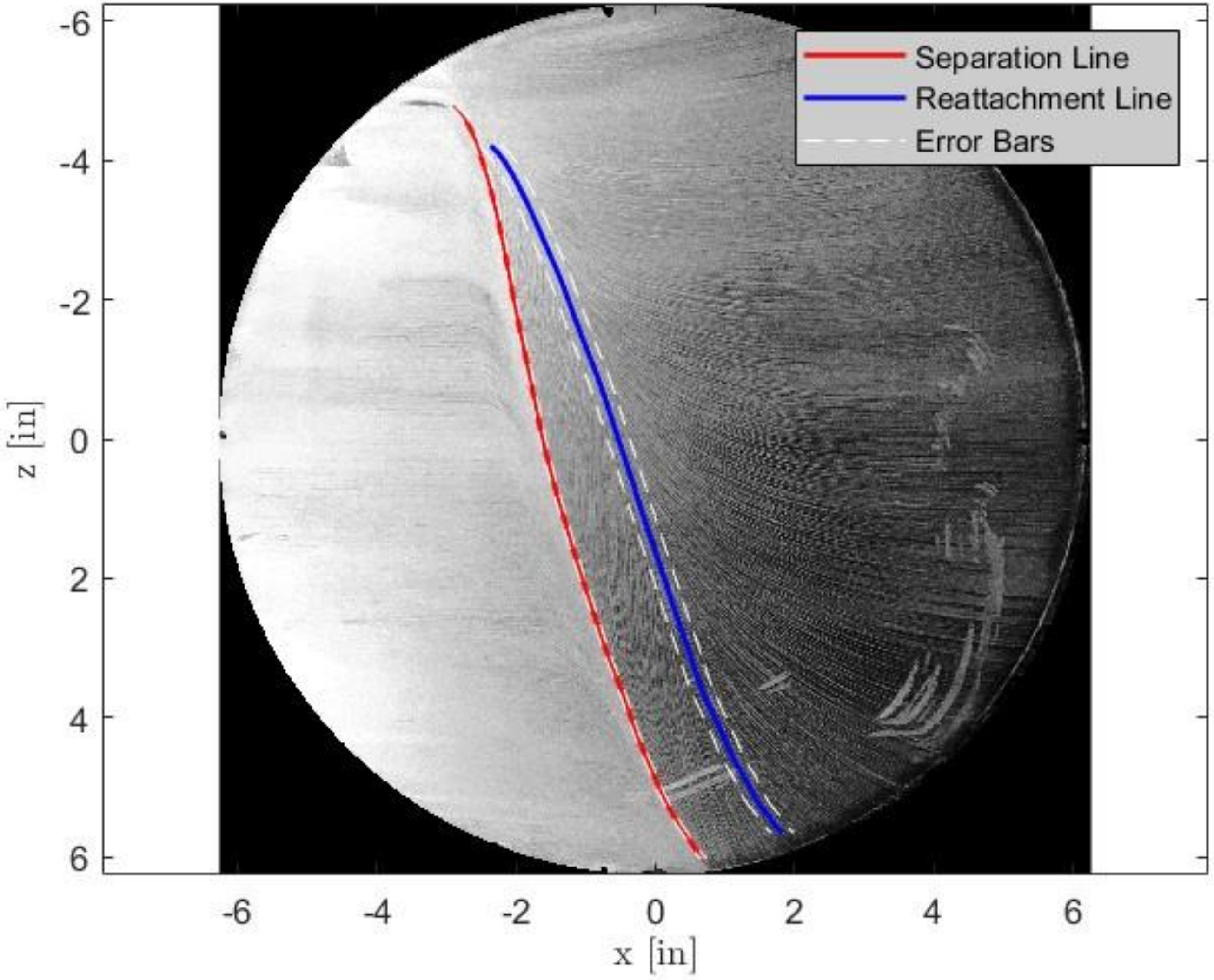

Oil Flow Results

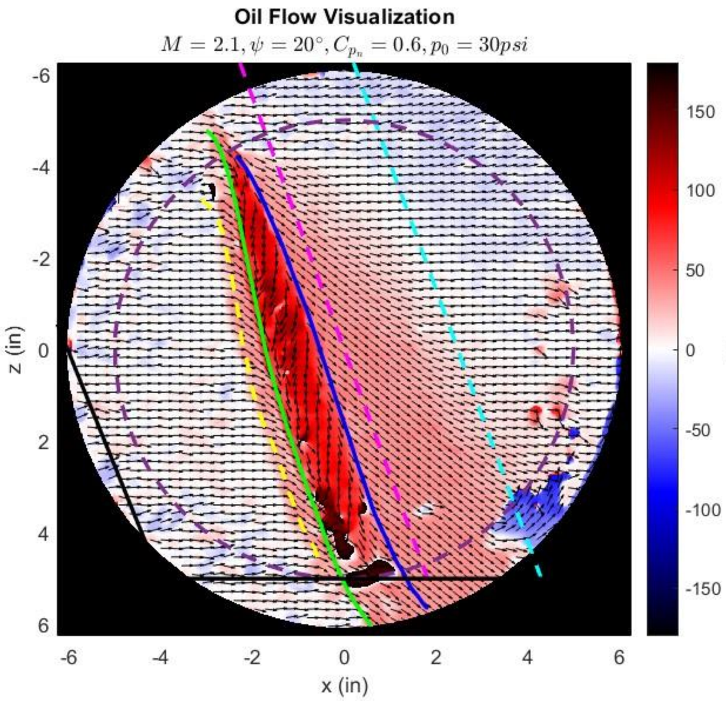

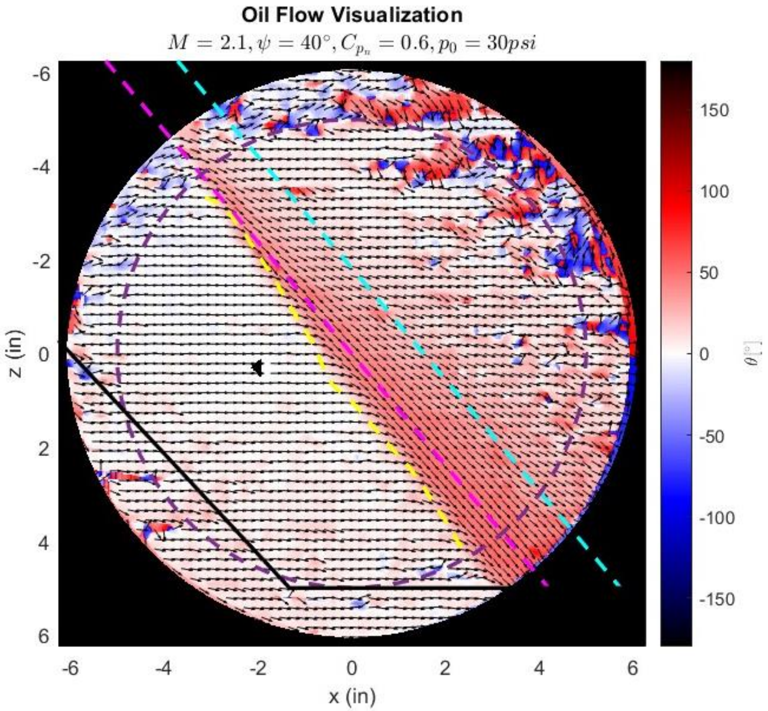

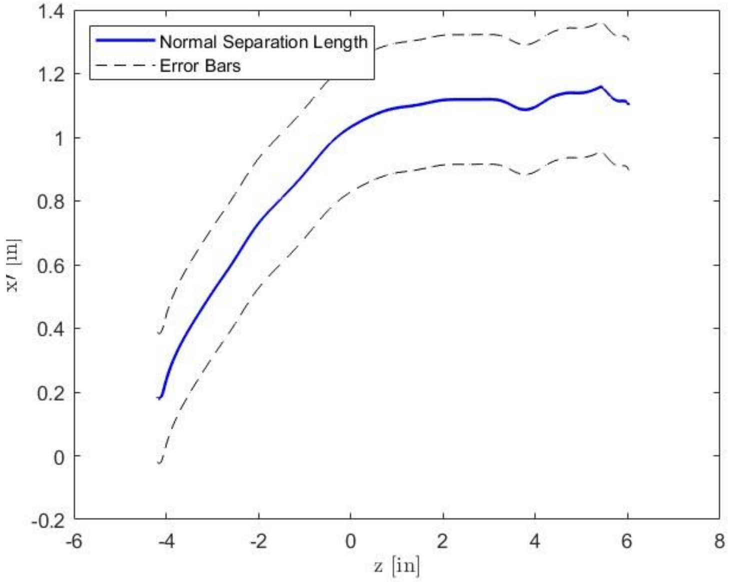

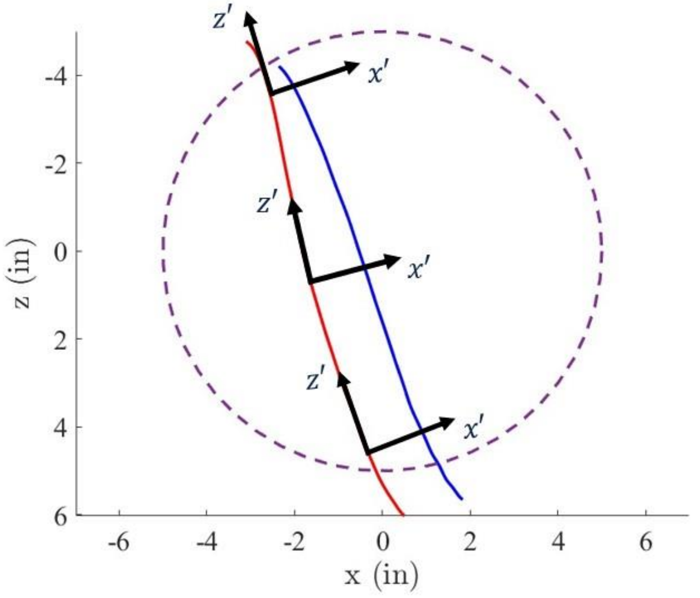

- Hand picked points align well with streak results
- Interaction becomes cylindrical around center of tunnel
- No sign of separation for 40° sweep
  - Expansion fan for this case is considerably closer than other cases

Region of Interest (ROI)

- Determined using mean pressure and oil flow results
  - Initial pressure rise used to determine angle of region
  - Oil flow determines maximum and minimum z values

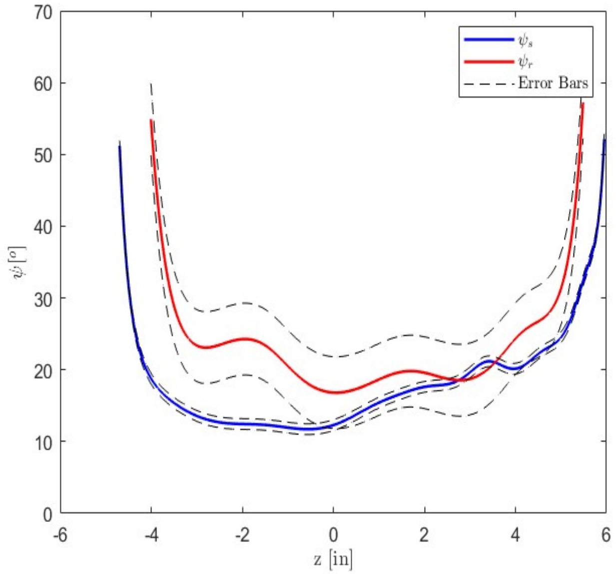

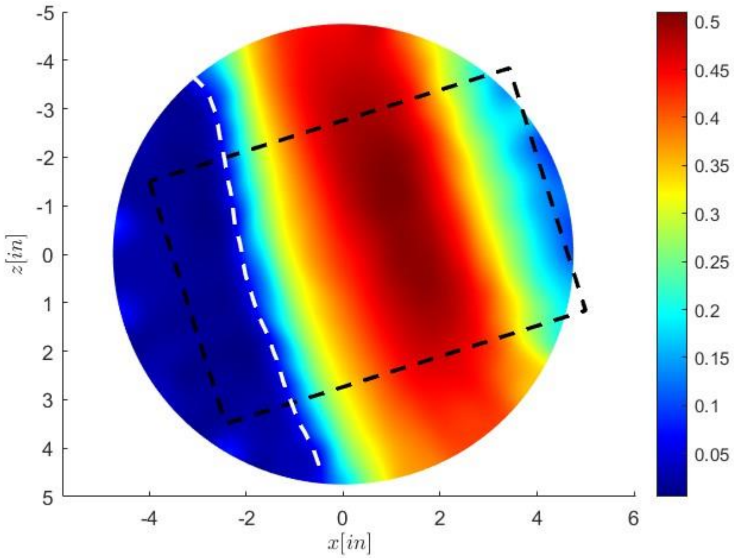

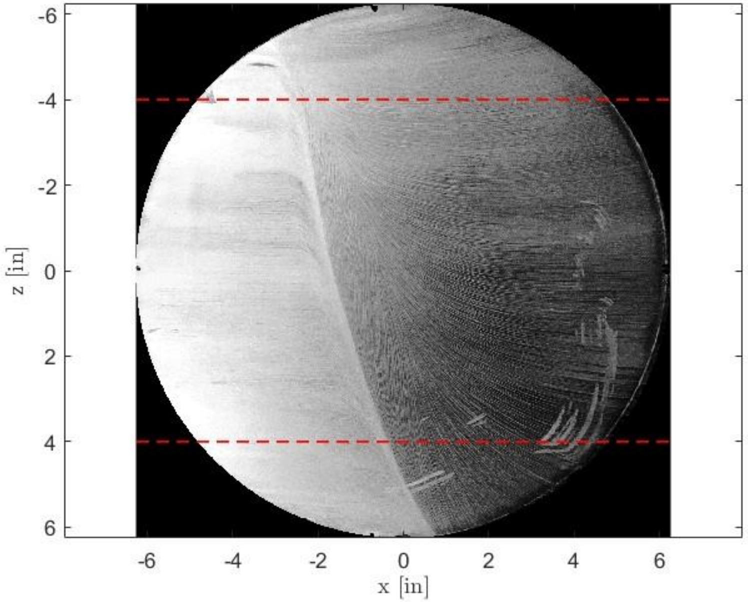

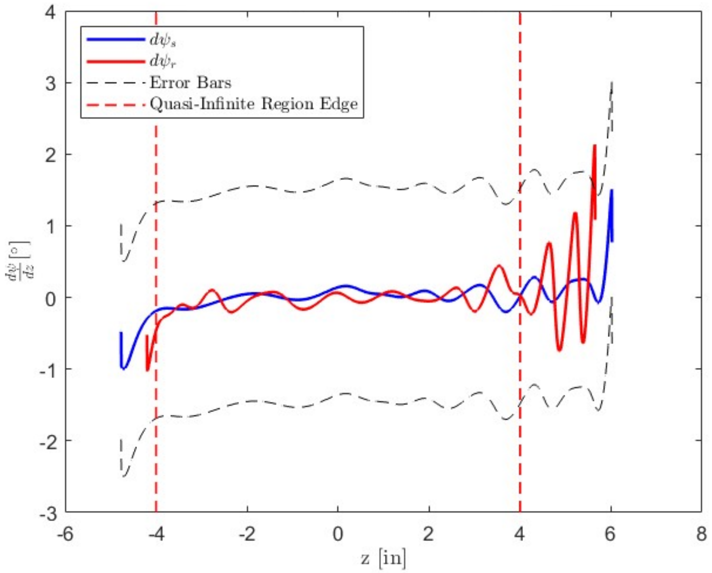

Mean Pressure

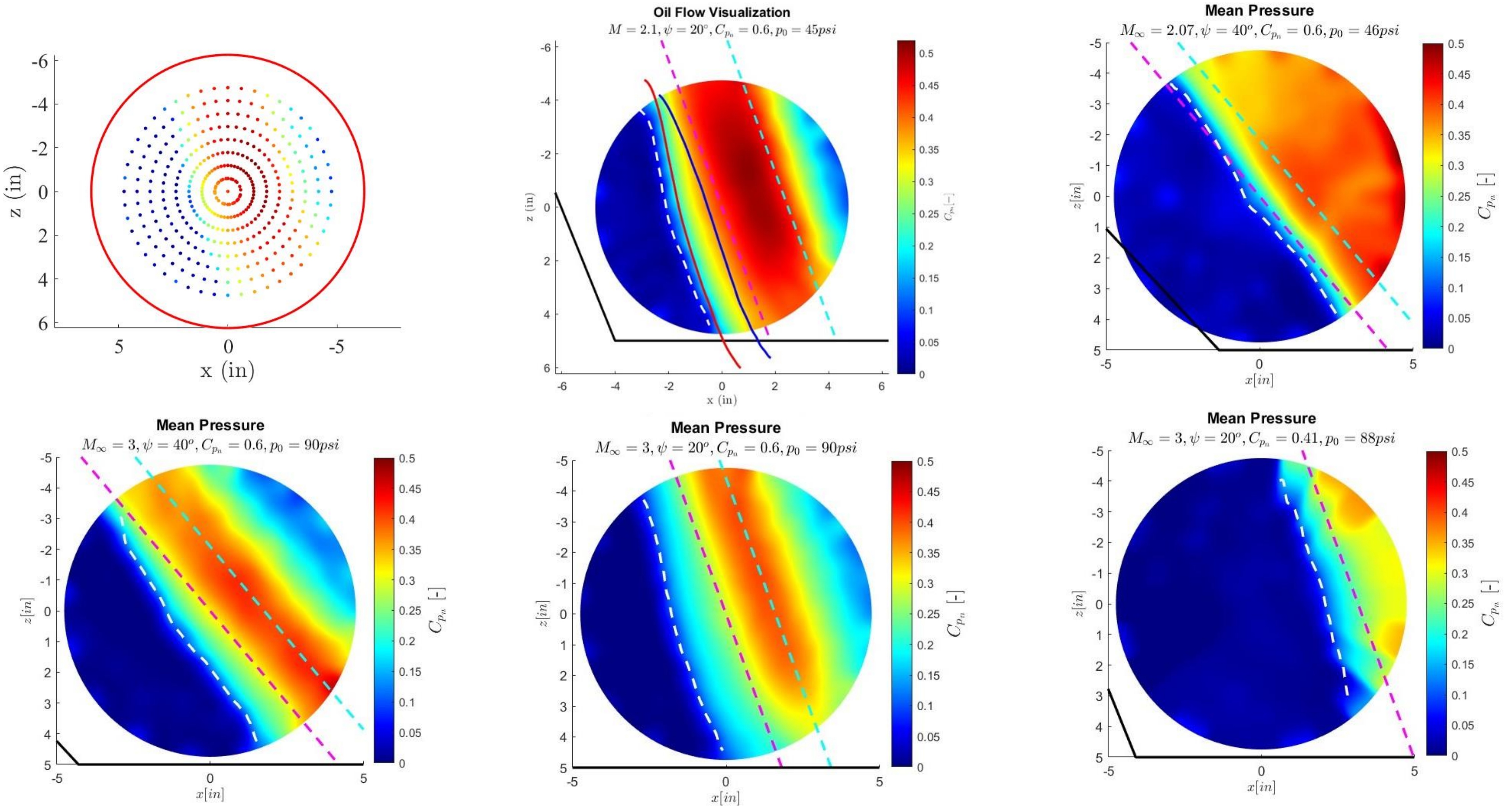

Mean Pressure Distribution: Constant Mach Number

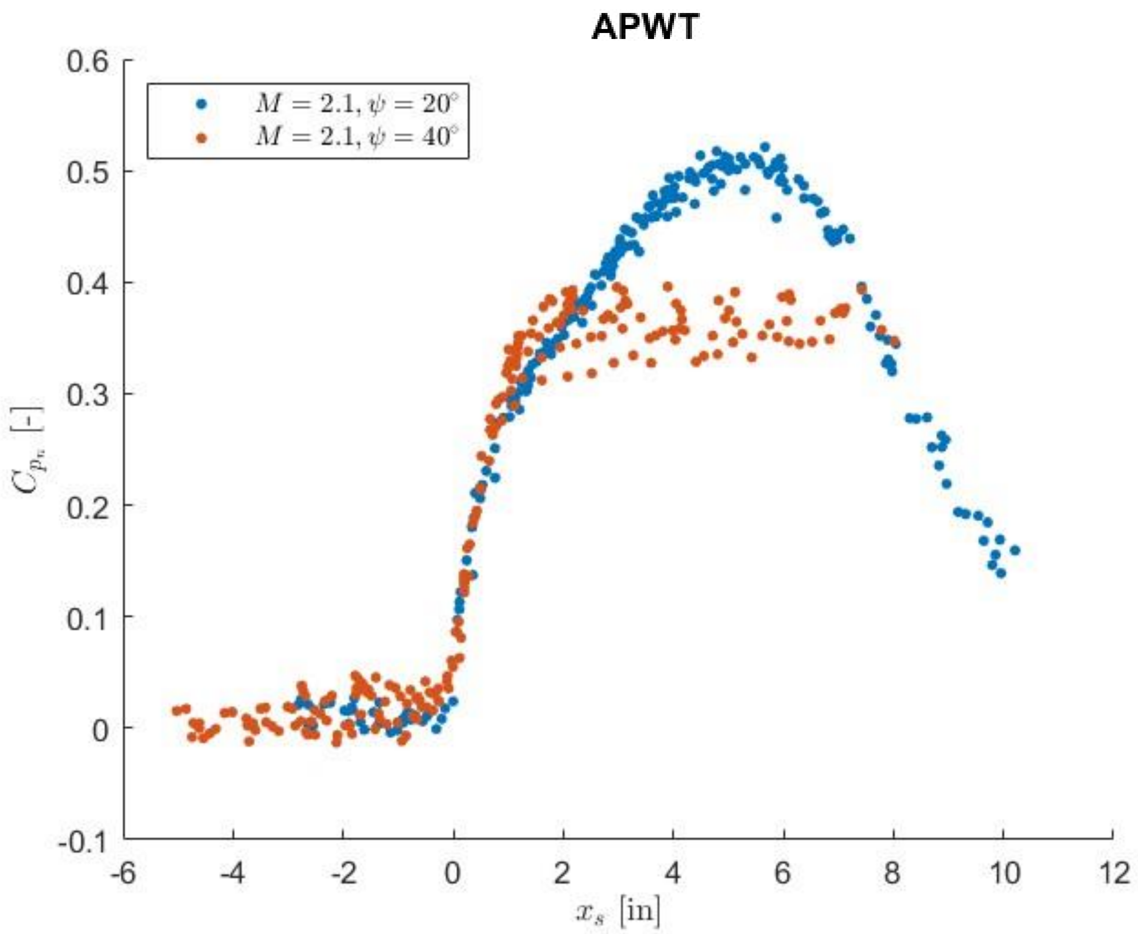

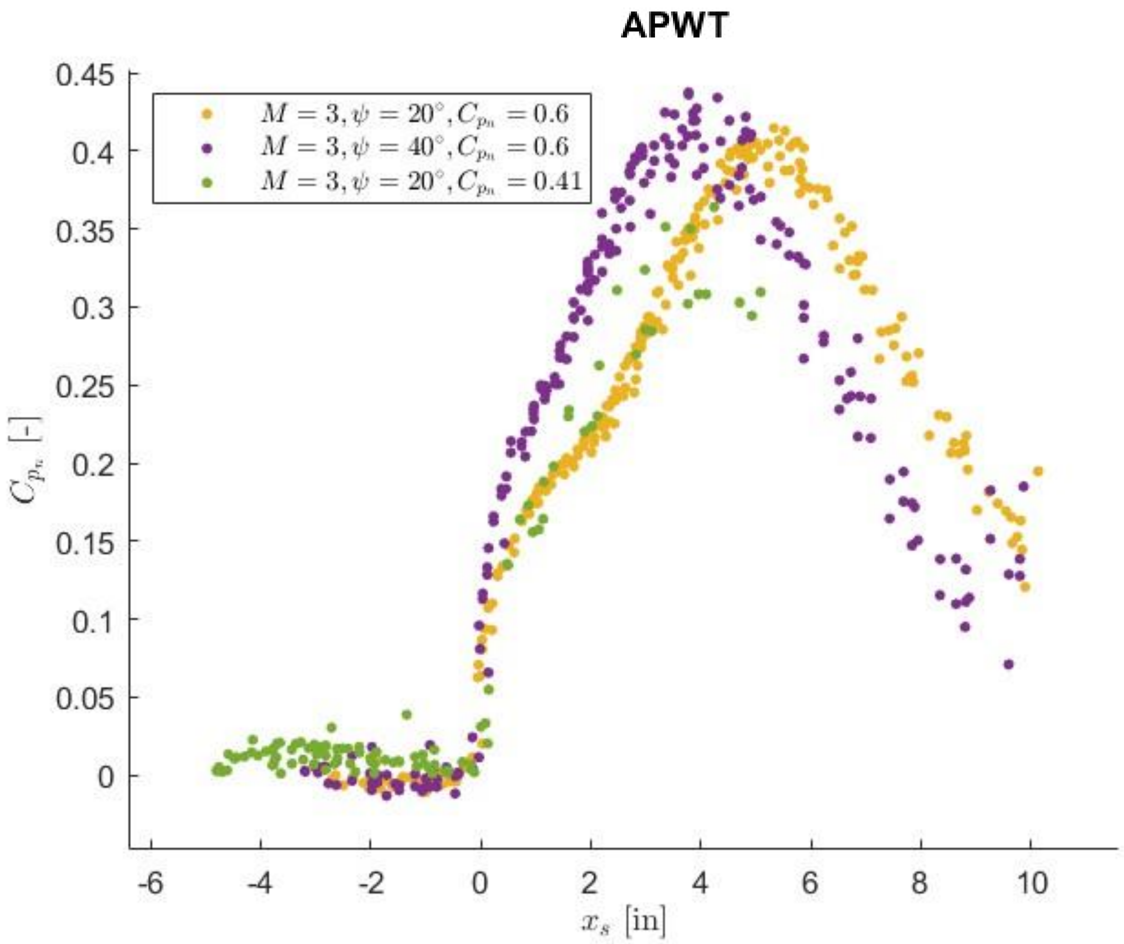

Mean Pressure Distribution: Constant Sweep

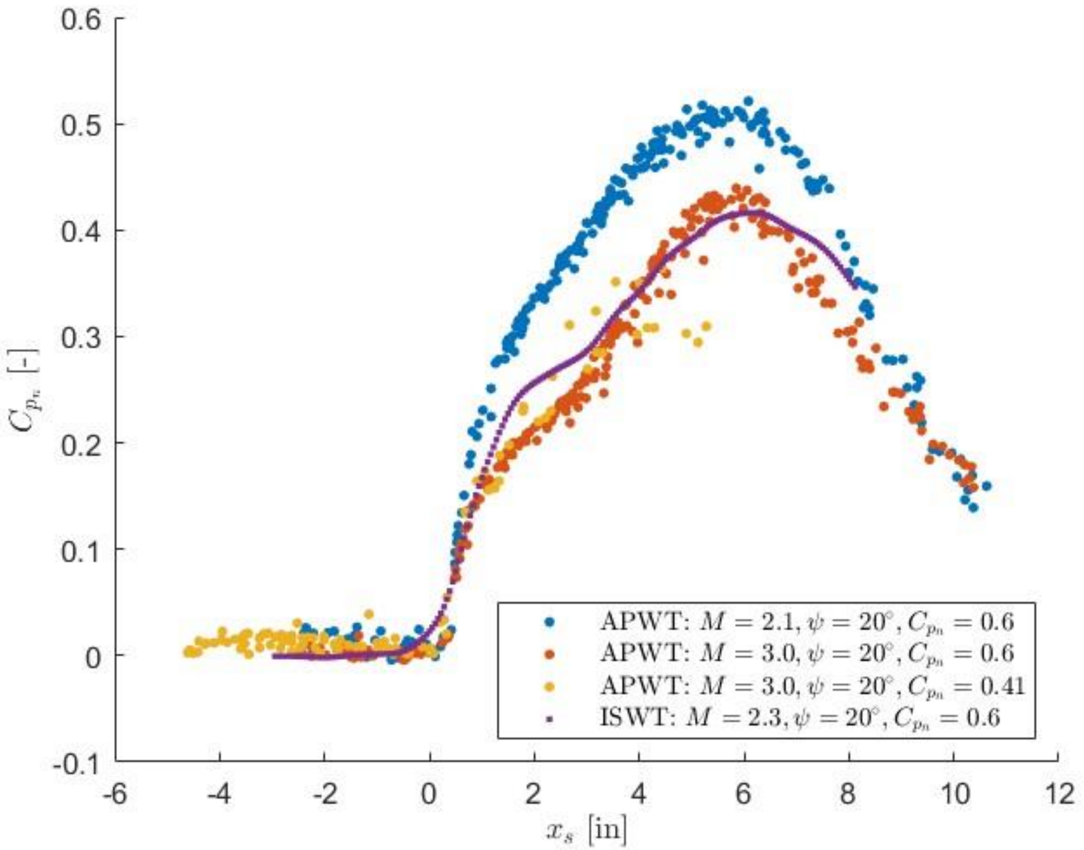

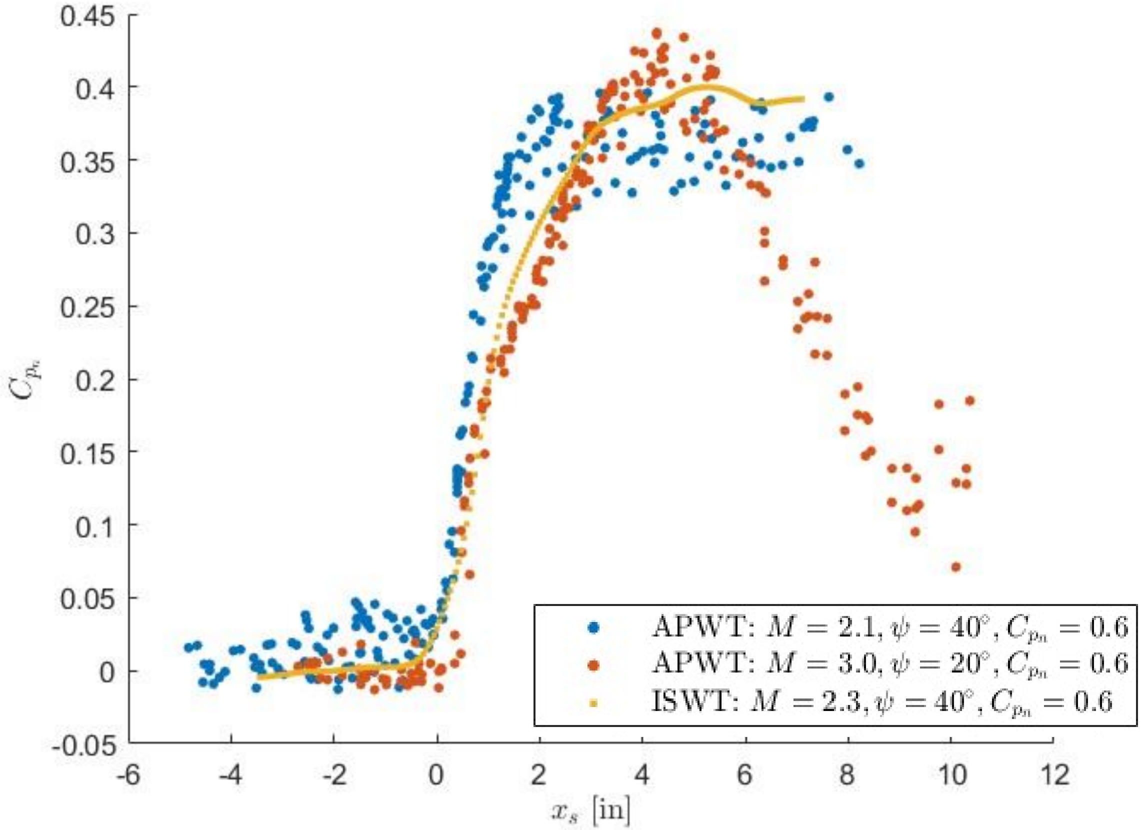

Infrared Results

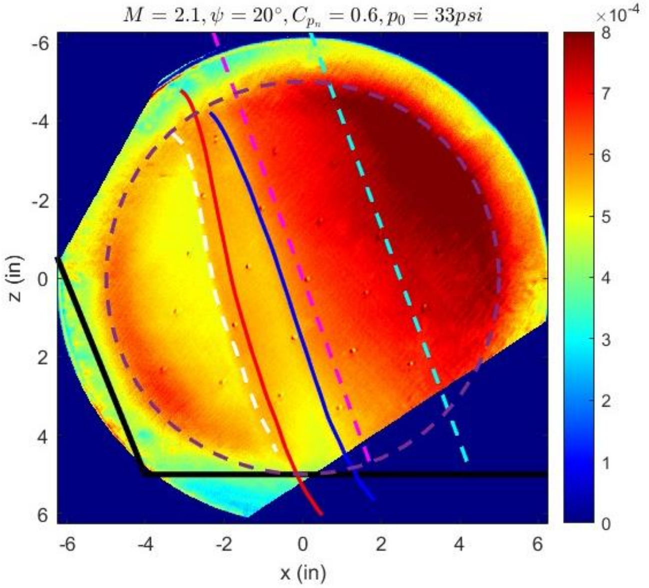

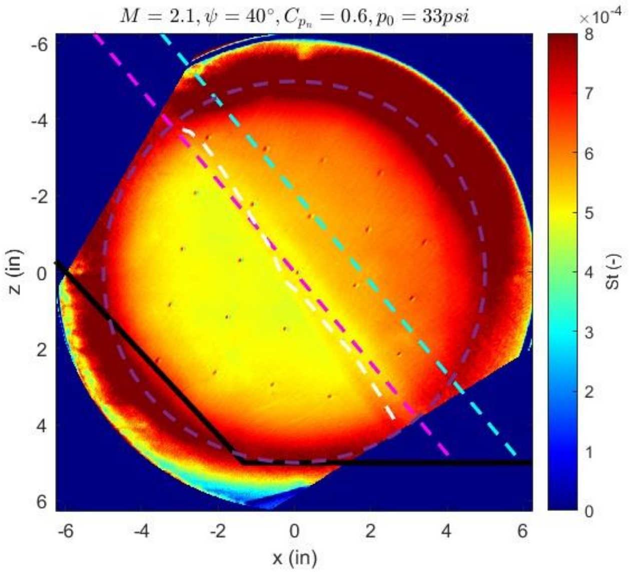

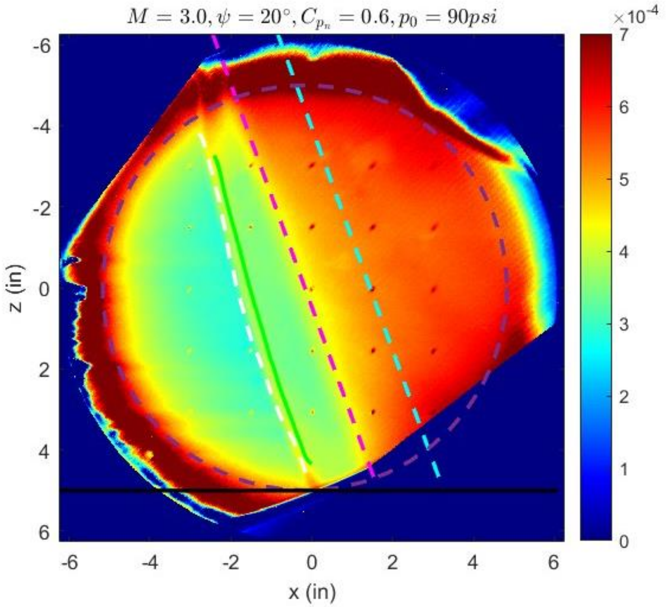

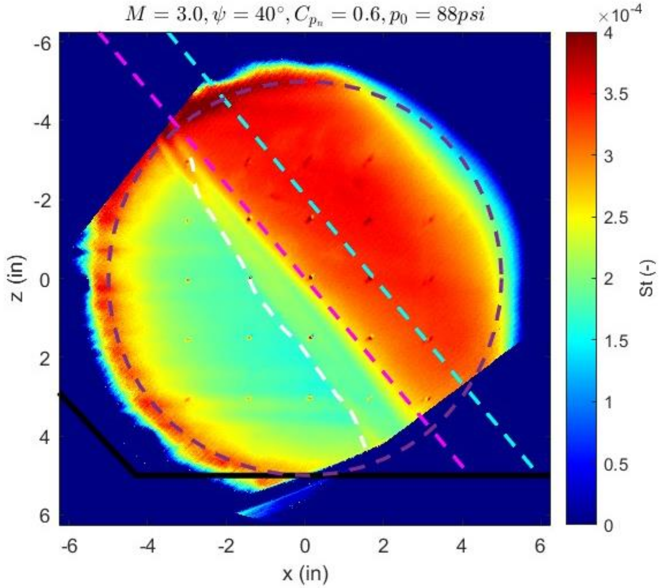

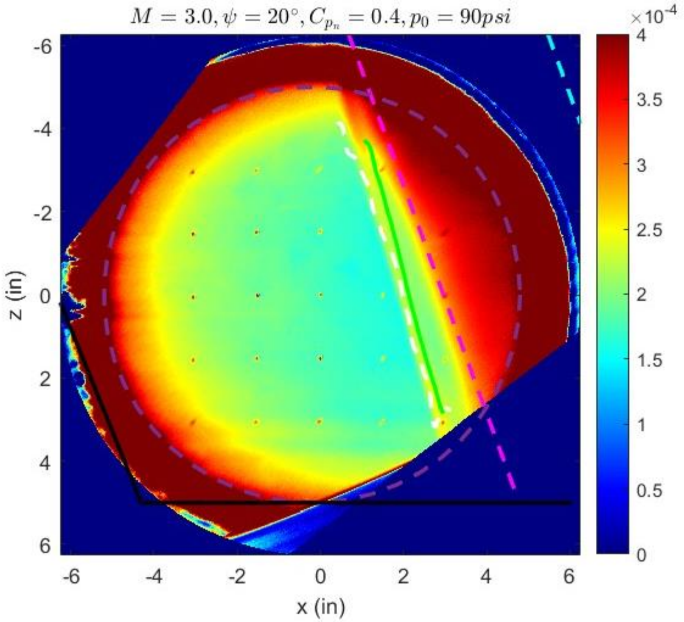

Initial Pressure Rise and Separation from Stanton Number

- Initial pressure rise and separation are extracted by plotting local minima and maxima
- Results show good agreement with oil flow (separation) and mean pressure (initial pressure rise)

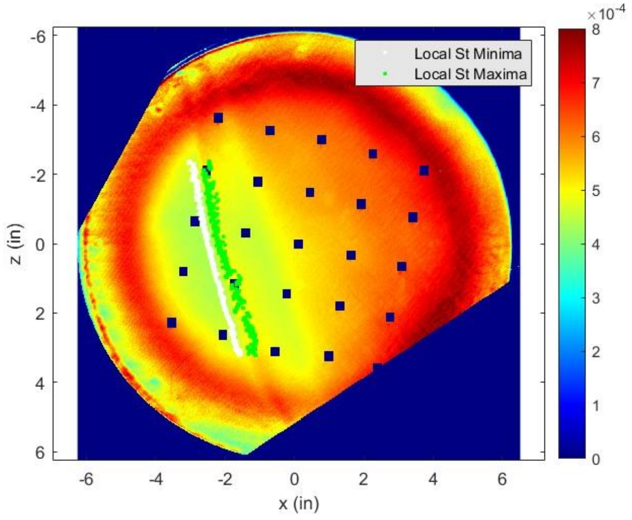

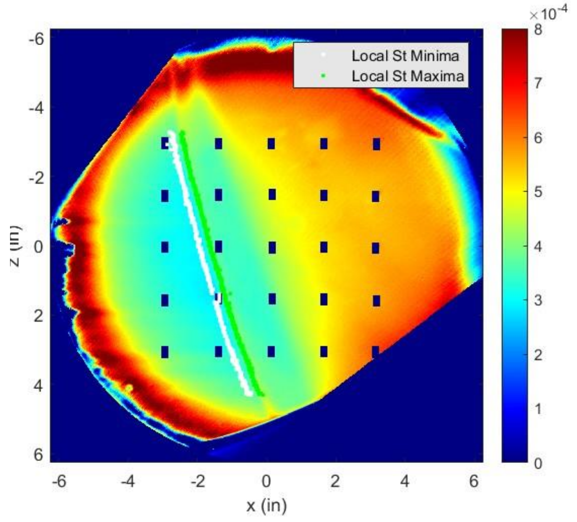

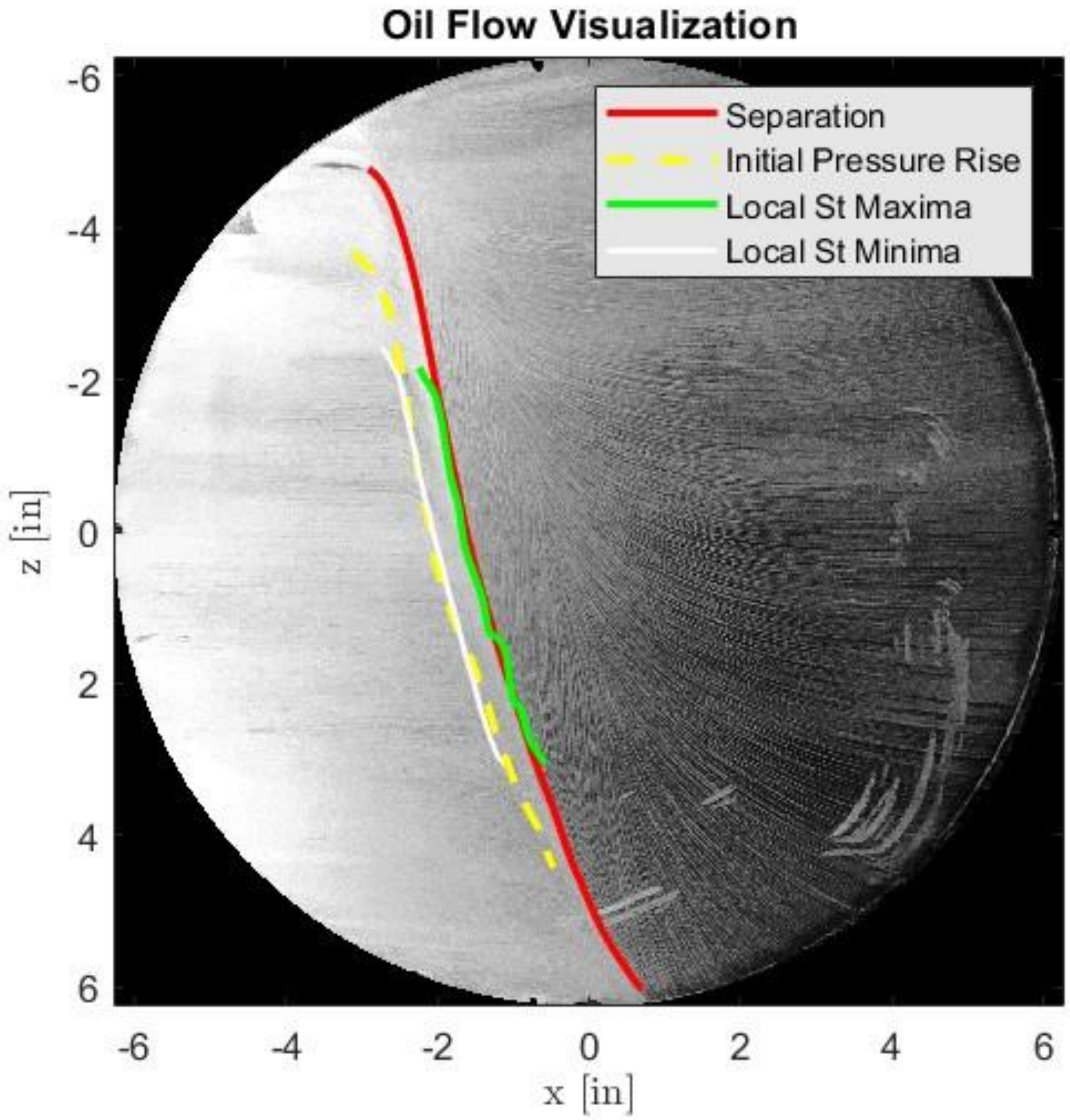

Region of Interest (ROI)

- ROI for to get Stanton number distribution is slightly different than mean pressure ROI
  - Only the center of mean pressure ROI used to avoid loss of features in Stanton number distribution
- Stanton number trace line determined using Gaussian kernel regression through points

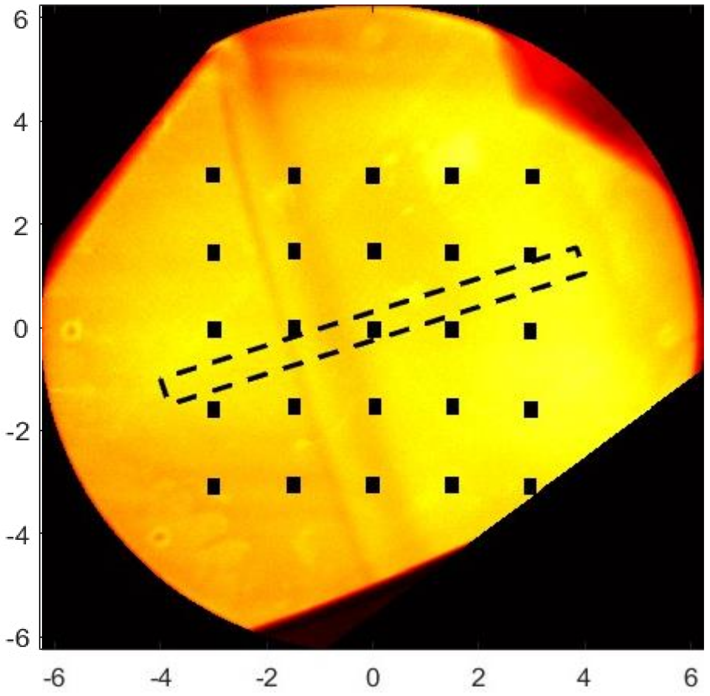

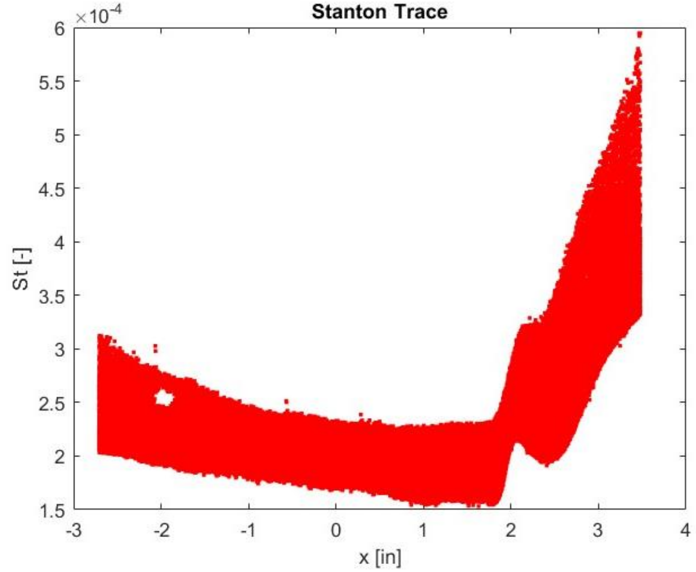

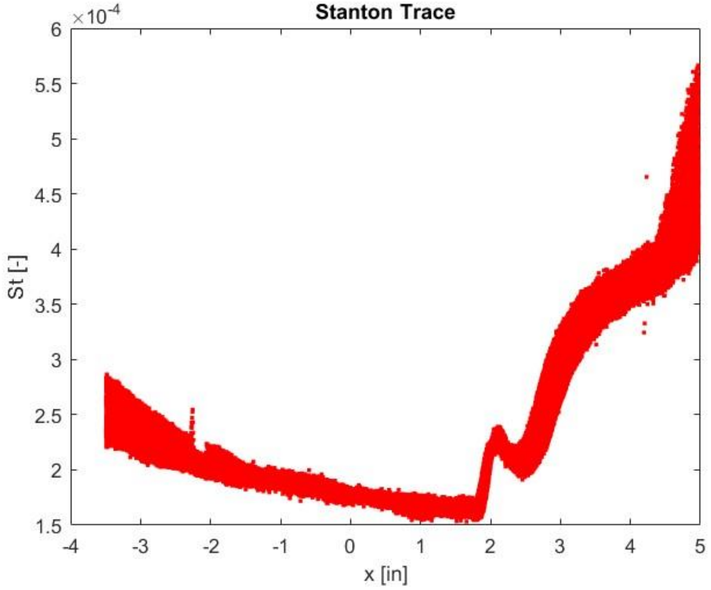

Stanton number and Mean Pressure Distribution Comparison

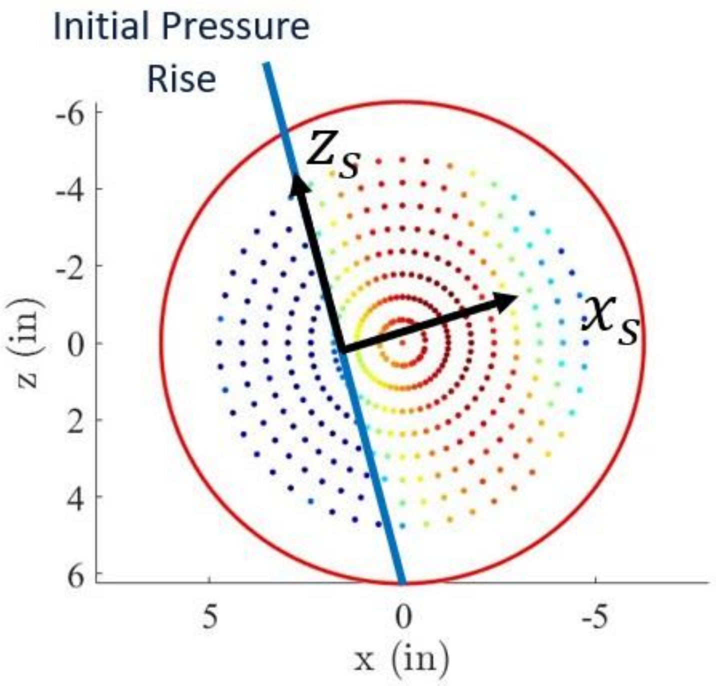

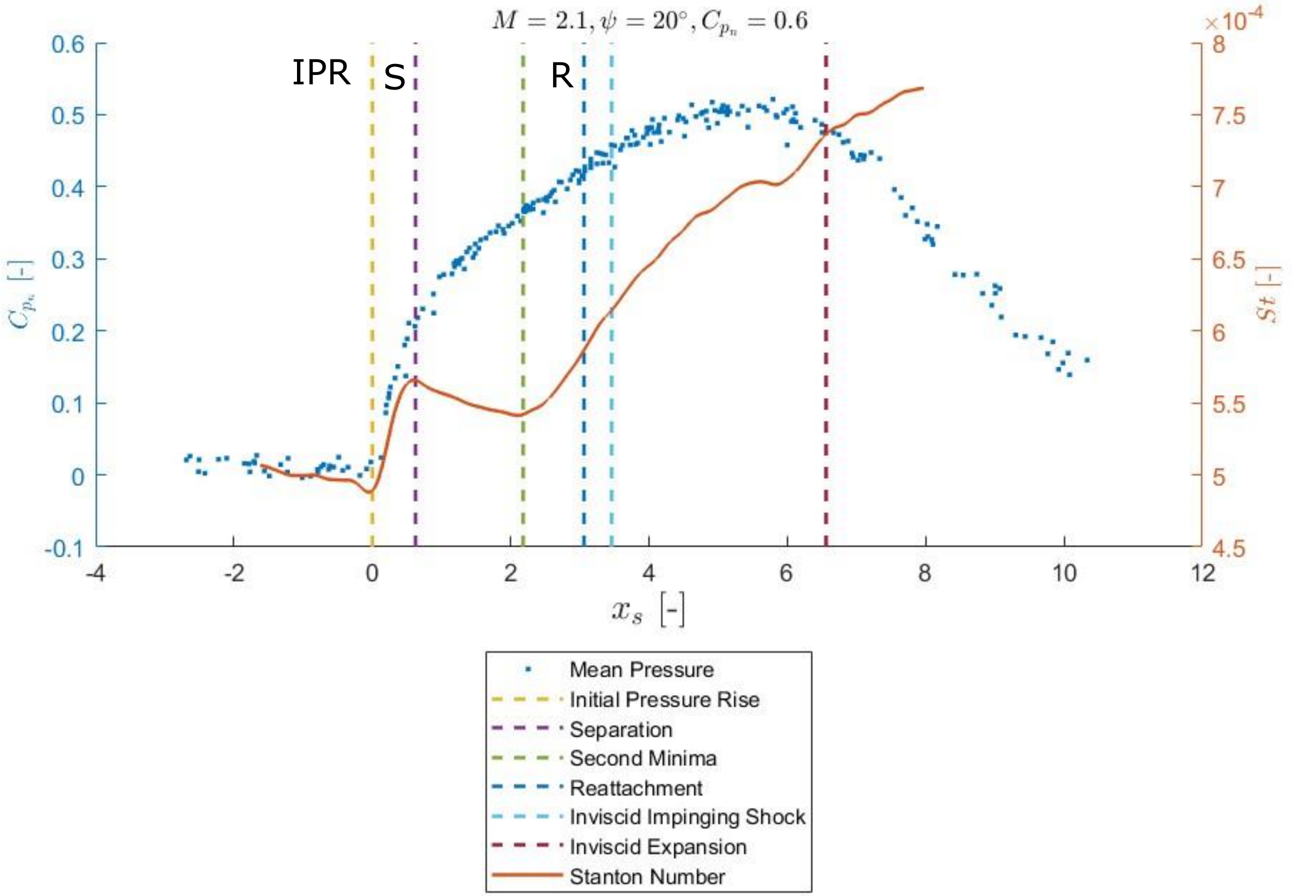

Stanton number and Mean Pressure Distribution Comparison

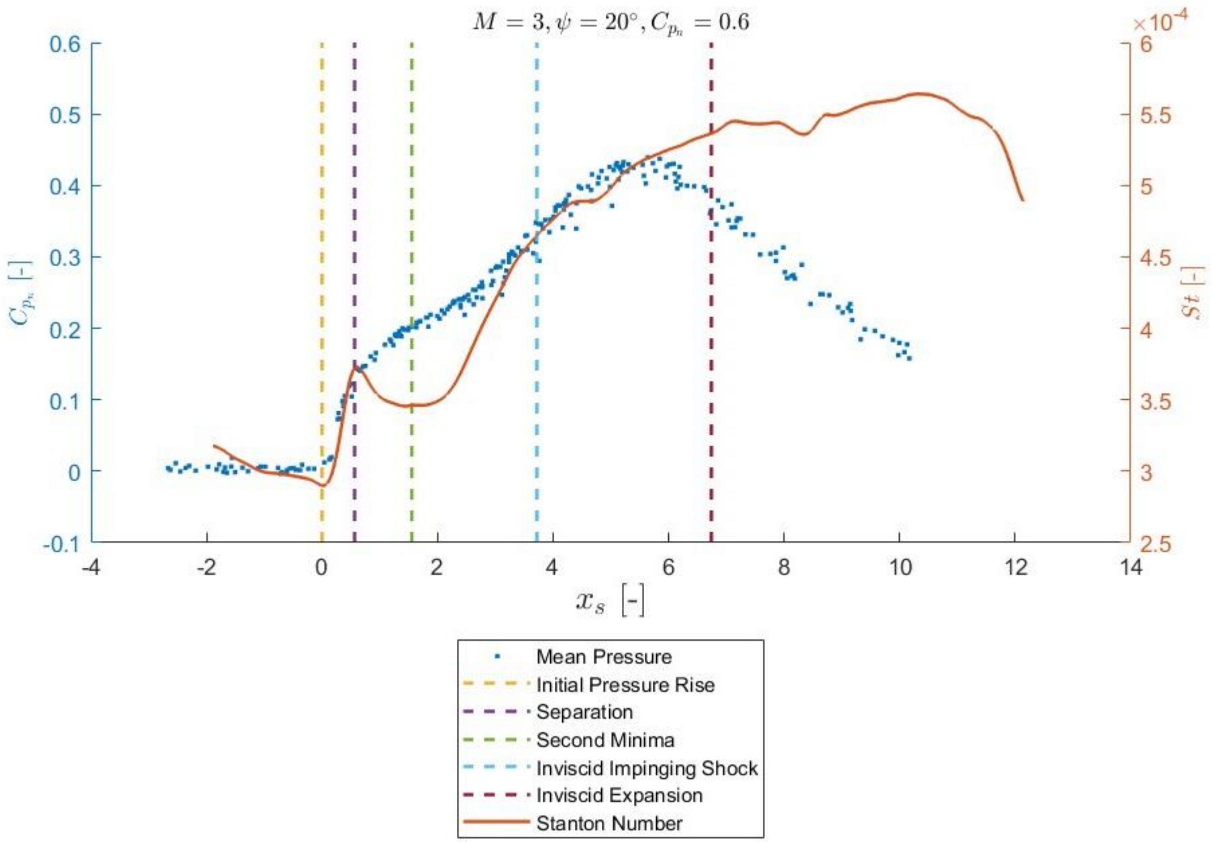

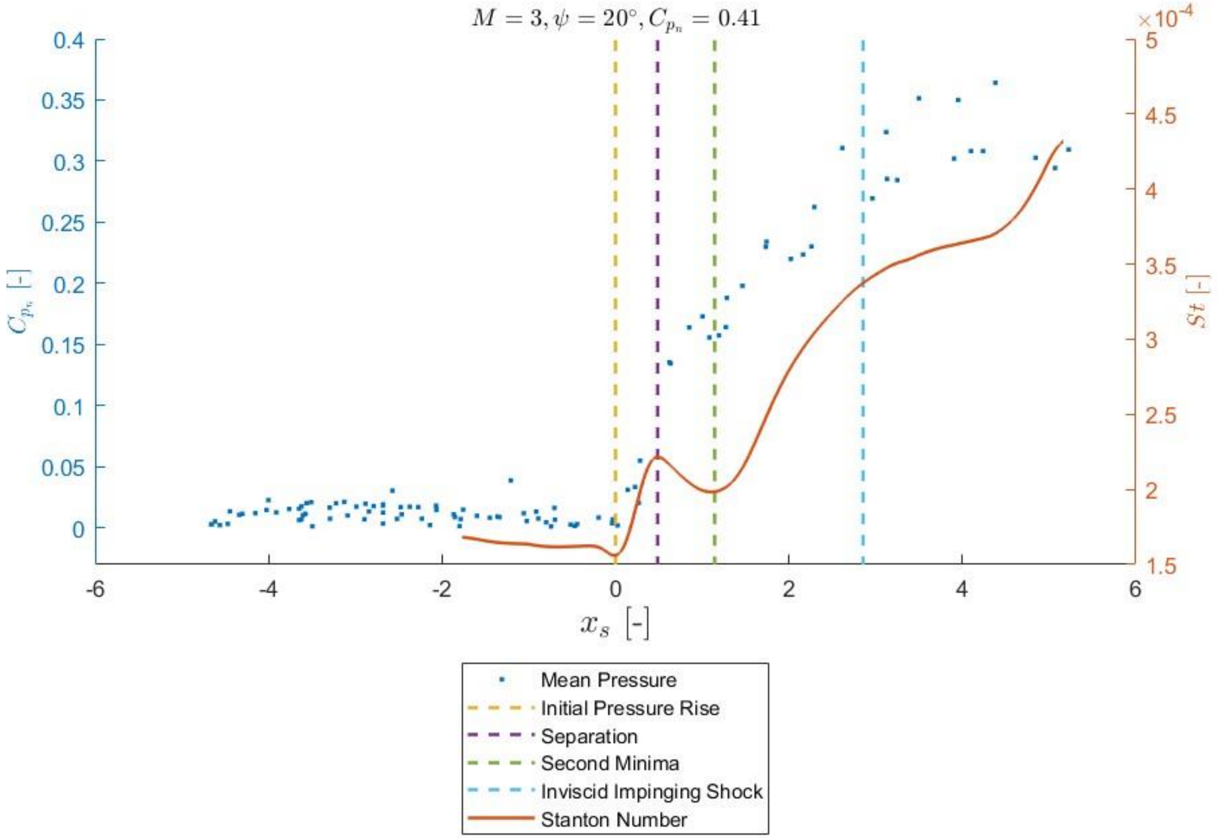

Stanton number and Mean Pressure Distribution Comparison

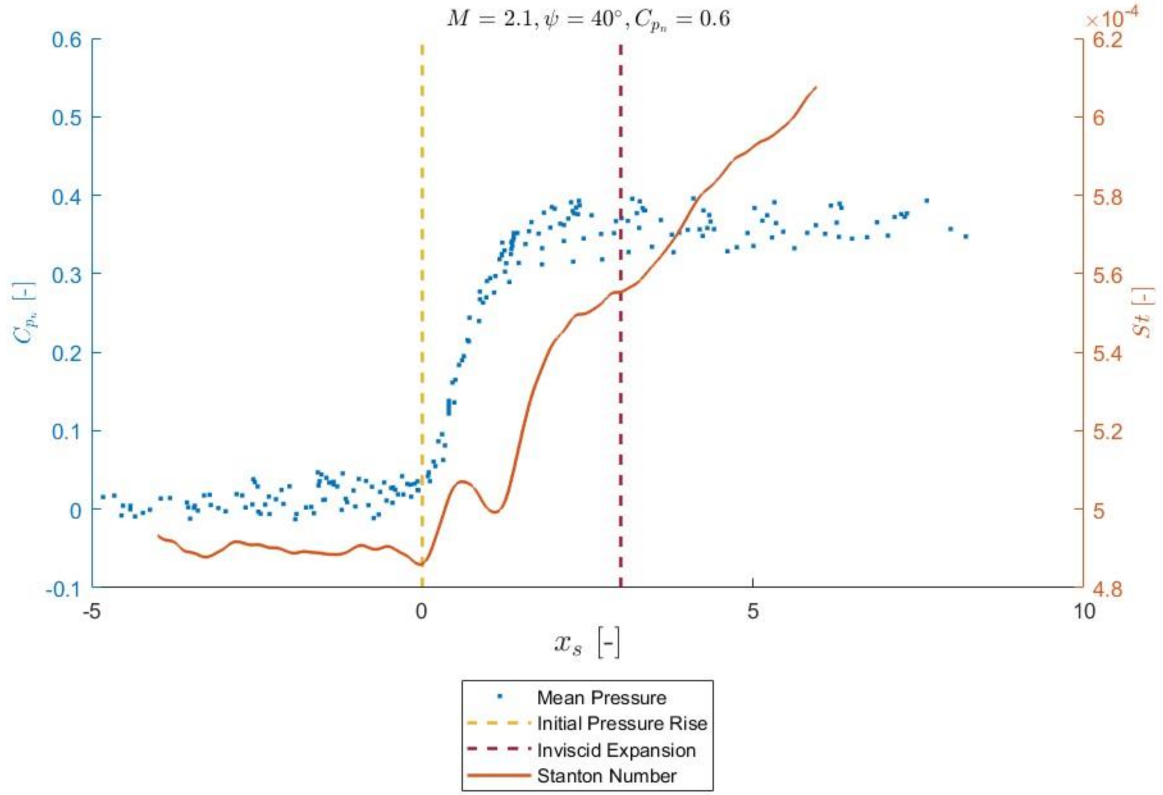

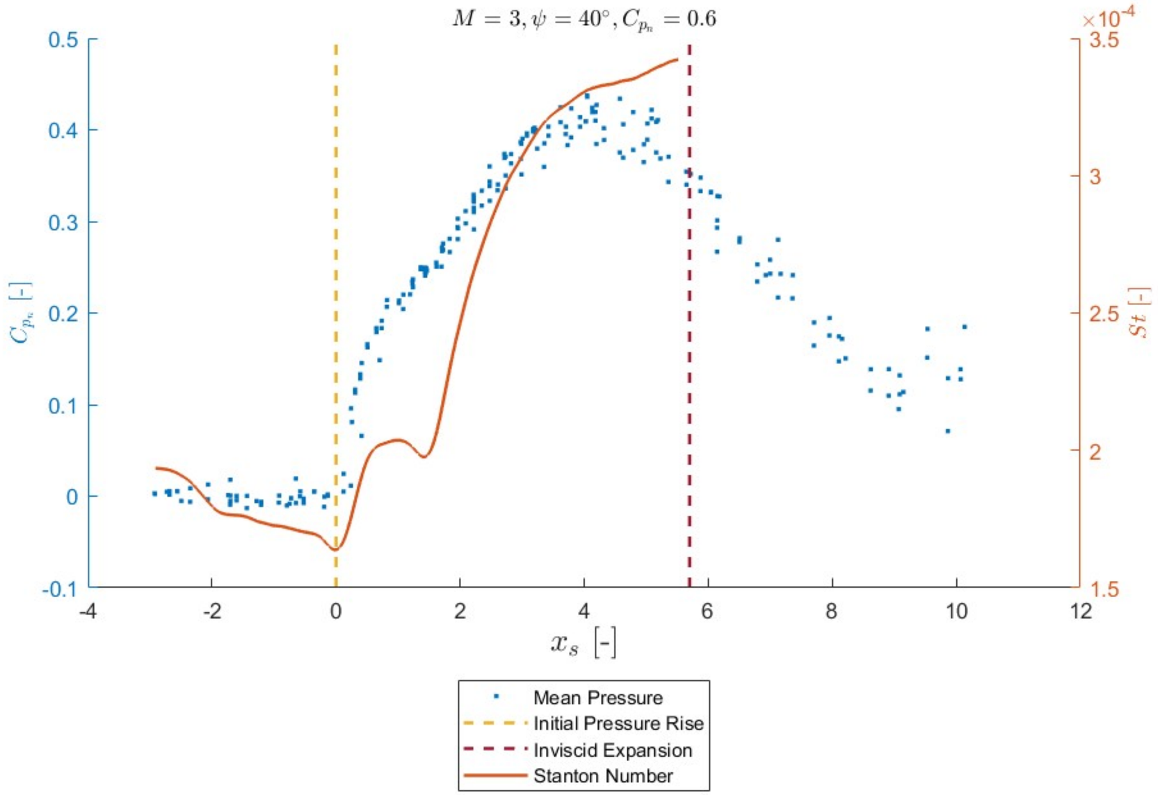

Conclusion

- Increase in Mach number decreases the initial pressure rise for similar sweep cases.
- Changing only the C_{p_n} appears to also show similar pressure rise for the initial part of the separated region which is in agreement with Free Interaction Theory.
- The boundary layer at the designed $C_{p_n} = 0.6$ is separated for a 20° sweep and attached for the 40° case
  - Threshold for separated flow likely over 30° based on data from ISWT
- Reynolds number has no discernable effect on the interaction which is consistent with results found by Souverein et al. (2013)
- Increasing aspect ratio suggests flow becomes cylindrical given large enough span.
- Scaling with the boundary layer height allows for comparison between ISWT and APWT.

Questions

Backup Slides

Oil Flow Results

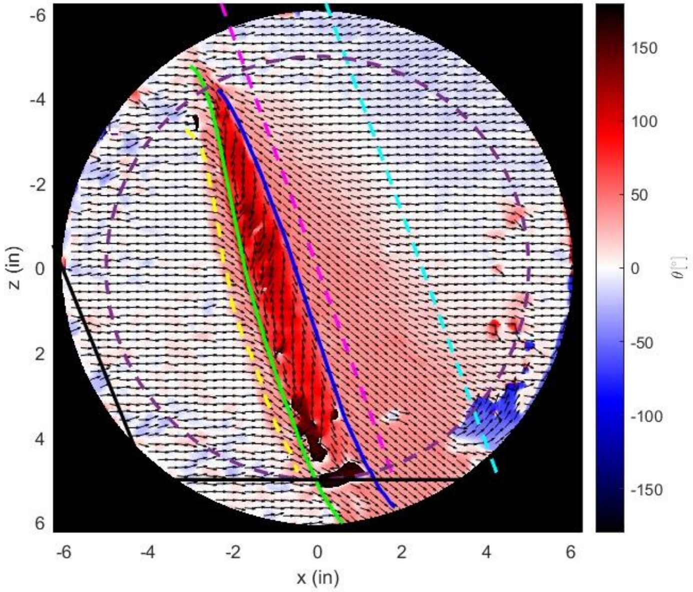

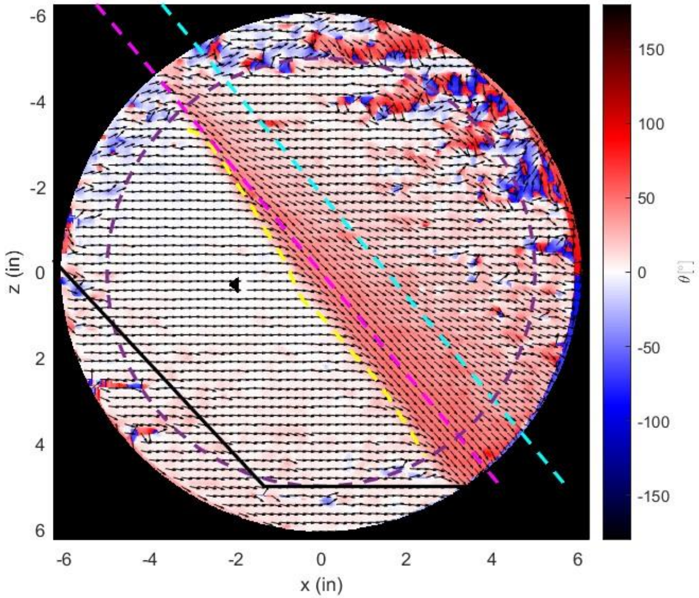

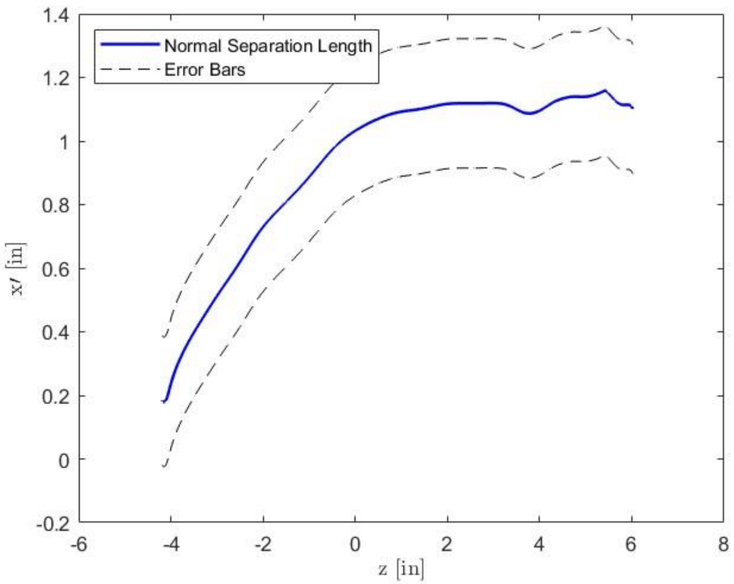

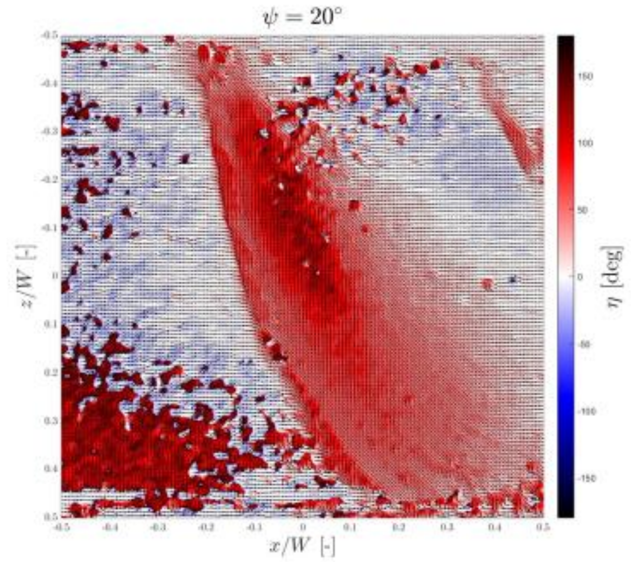

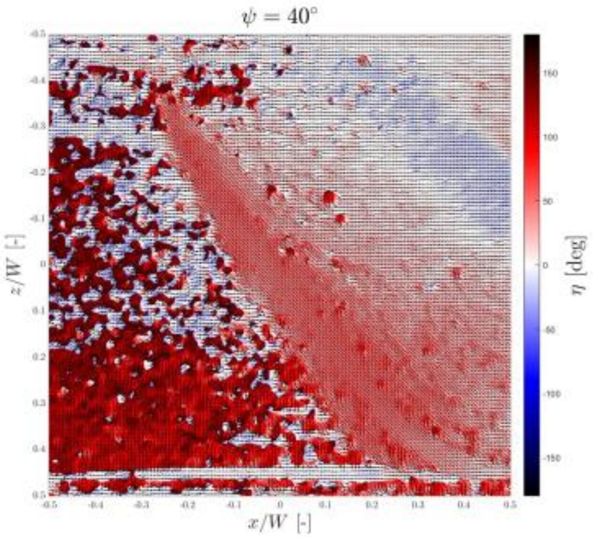

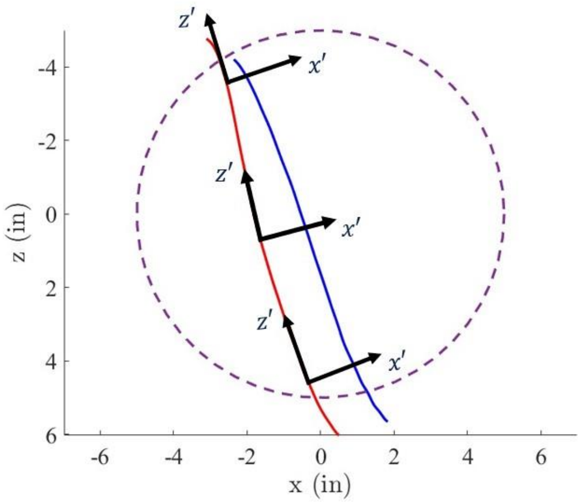

Determination of Initial Pressure Rise Location

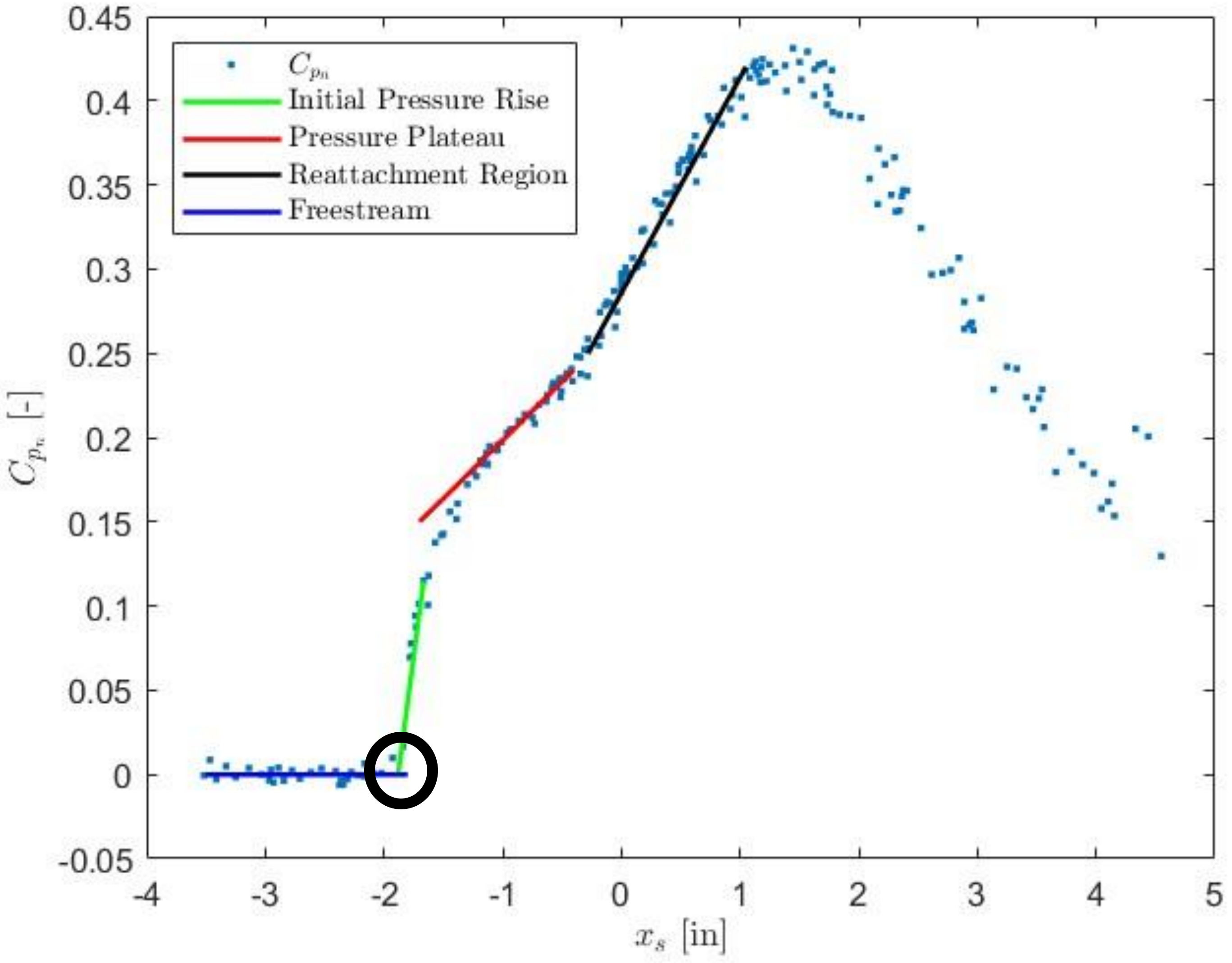

Initial Pressure Rise and Separation Comparison